Republic of Iraq
Ministry of Higher Education
and Scientific Research
Babylon University / College of Engineering
Department of Civil Engineering

Behavior of Non-Prismatic Reinforced Concrete One Way Slabs under Repeated Load

A Thesis
Submitted to the College of Engineering at University of Babylon in Partial Fulfillment of the Requirements for the Degree of Master in Engineering/ Civil Engineering/ Structures Engineering

By
Fatima Neama Ibrahim Mseer
B.Sc. Civil Engineering, 2017

Supervised by
Prof. Dr. Nameer A. Alwash

2022

بسم الله الرحمن الرحيم

﴿قَالُوا سُبْحَانَكَ لَا عِلْمَ لَنَا إِلَّا مَا عَلَّمْتَنَا إِنَّكَ أَنْتَ الْعَلِيمُ الْحَكِيمُ﴾

صدق الله العلي العظيم

سورة البقرة - الآية (٣٢)

Certificate

I certify that **Fatima Neama Ibrahim Mseer** accomplished the preparation of this thesis entitled "**Behavior of Non-Prismatic Reinforced Concrete One Way Slabs under Repeated Load**" under my supervision at the University of Babylon in fulfillment of partial requirements for the Degree of Master in Engineering/ Civil Engineering/ Structures Engineering

Signature:

Name: Prof. Dr. Nameer A. Alwash

Certificate of the Examining Committee

We certify as an Examining Committee that we have read this thesis entitled "**Behavior of Non-Prismatic Reinforced Concrete One Way Slabs under Repeated Load**", and examined the student Fatima Neama Ibrahim Mseer in its content and in what is related to it. We found that, it meets the standard of thesis for the Degree of Master in Engineering/ Civil Engineering/ Structures Engineering

Signature:
Name: **Prof. Dr. Nameer A. Alwash**
(Member and Supervisor)

Signature:
Name:
(Member)

Signature:
Name:
(Member)

Signature:
Name:
(Chairman)

Approved by The Head of the Civil Engineering Department

Signature:
Name: Prof. Dr. Thair Jabbar Mizhir
(The Head of the Civil Engineering Department)

Approved by the Dean of the Engineering College

Signature:
Name: Prof. Dr. Hatem Hadi Obeid
(The Dean of the College of Engineering)

Dedication

To my parents

To my beloved husband

To every member in my family

To my supervisor Prof. Dr. Nameer A. Alwash

With respect

Acknowledgments

In the name of Allah, the most gracious, the most merciful

All thanks and praise to Allah who enabled me to achieve this research work. Firstly, I would like to express my sincerest gratitude to my supervising, Prof. Dr. Nameer A. Alwash, for his invaluable insight, wisdom, and guidance

I would like to thank the support staff of the Department of Civil Engineering of Babylon University for their assistance with daily matters throughout my graduate academic life.

I would like to acknowledge the friendly support and assistance of my fellow graduate students who made my overall experience more gratifying.

Finally, a special thanks and gratitude to my family for their care, and patience, who have been by my side throughout this entire endeavor. Without their love, encouragement, and support I would not have been able to complete this academic achievement.

Fatima Neama Ibrahim Mseer

2022

Abstract

This research presents an experimental and numerical investigation of the behavior of non-prismatic RC one-way slabs under repeated load. The experimental work consisted of testing eleven reinforced concrete one-way slabs divided into two groups. The first group consists of five slabs with one span, while the second group included six slabs with two spans. The effects of three parameters on the overall behavior of slabs were studied, including; tapering configuration, support condition and number of spans.

For slabs of the first group, one of them were prismatic with constant depth, while, all the others were non-prismatic with tapered cross section have varying depth and different boundary conditions with the same volume of concrete and steel. The results indicates that, the load capacity for simply supported one-way slab with positive haunch increases by 32% with related to prismatic slab. While it increased by 68 % for clamped slab with negative haunch.

On the other hand, slabs of the second group consisted of fabrication and testing six two span RC slabs with the same volume of concrete. Two of them were prismatic with constant depth, while, all the others were non-prismatic with tapered cross section have varying depth. The results indicates that, in all support condition prismatic slabs were somewhat stiffer than non-prismatic slabs. It is found that providing tapered slab with positive or negative haunch have insignificant effect on the bearing capacity with respect to prismatic slab. On the other hand, it caused increase in the deflection at service load compared to prismatic slab. Thus, it is recommended to use prismatic continuous one-way slabs rather than non-prismatic ones because of higher stiffness and almost the same load carrying capacity.

In the second part of this study, a three-dimensional finite element model, using the concrete damaged plasticity model and material properties obtained from laboratory tests was conducted to simulate reinforced concrete slabs within a

commercial finite element software package ABAQUS/standard 2017. Numerical results are compared with the obtained experimental results. It is found that, 3D finite element analysis, based on the CDP model by ABAQUS package is valid for the analysis of RC slabs. The general response of load-deflection curves, the ultimate load, and the mid span deflection of the studied reinforced slabs predicted by FEM were in good agreement with the experimental results. The average difference in results was about 5.9% increase in ultimate loads, a 5.37 % decrease in the maximum deflection at service loads, and a 4.1% increase in the maximum deflection at ultimate loads. Numerically, repeated load protocol that adopted experimentally and numerically was proved to be effective in study the adverse effect of applying repeated load in comparison with monotonic load.

List of Contents

List of Tables

List of Figures

1

Chapter 1
INTRODUCTION

1.1 General

A slab is described as an essential member for constructing reinforced concrete building and it is frequently created using monolithic reinforced concrete. The structural behavior of reinforced concrete slabs is evaluated by the strength requirements alongside with the serviceability limit state. This might be improved by increasing the slab stiffness (increasing the slab thickness), utilizing full or partial pre-stressed reinforcement, or using high strength concrete (HSC).

Using pre-stressed reinforcement is taken into account a rather complicated process since it requires high labor costs and expensive equipment. Therefore, increasing the thickness of ferroconcrete slabs is more preferable choice to increase the stiffness. Unfortunately, increasing the thickness of the concrete slab could cause increasing the slab weight alongside reducing the useful space between floors. So, using non-prismatic slabs may reduce the slab weight with sufficient stiffness.

Large reductions in embodied carbon can be achieved through the optimization of concrete structures. Such structures tend to vary in depth along their length, creating new challenges for flexure and shear design. In the last decades, intensive research has been conducted on the effect of using non-prismatic cross section on the behavior of RC structural elements. The researchers have focused mainly on RC beams with tapered cross section. These beams can provide steel and

concrete savings when used to replace equivalent strength prismatic elements (see Figure 1-1). In fact, non-prismatic slabs no less important, especially if they have benefits that can be utilized from. Therefore, studying the performance of tapered slabs is very important and is the main objective of this thesis.

Figure 1-1: Liuguanghe Bridge, Guizhou, China, Image by Eric Sakowski / HighestBridges.com

1.2 Non-Prismatic Reinforced Concrete Members:

Non-prismatic members are members with non-constant cross-section along their length. Despite the benefits that engineers can obtain from their use, non-trivial difficulties occurring within modeling this type of members often cause inaccurate predictions that vanish the gain of the optimization process. As a consequence, an efficient non-prismatic member modeling still represents a branch of the structural mechanics where significant improvements are required [1].

Because the structural engineering techniques were improved, non-prismatic members became utilized in various structures including buildings and bridges. With the members being tapered, the architects would be ready to create and implement novel aesthetic architectural designations, also the structural engineers who could search for optimum low weight - high strength systems through a redistribution of materials along the structural members [2].

Shape optimized concrete members use less concrete material than their prismatic counterparts because their shape reflects the wants of the loading resistant. Such members, generally have smaller cross-sectional dimensions along their length than the same strength prismatic one [3]. However, this makes them significantly less stiff and, in many cases, serviceability criteria instead of strength can govern their design [4]. Therefore, understanding the serviceability behavior of non-prismatic reinforced concrete members is vital.

Traditional formwork methods for concrete are used for prismatic building elements (such as beams, floors and columns), not because members must be prismatic to support its load, nor because it's difficult to shape concrete to other forms, but because existing fabrication techniques believe easy-to-construct prismatic molds. 30-50% of the concrete for some member is merely there due to the prismatic formwork it had been made in. For too long, the industry has used "ease of construction" as an excuse to waste material [5].

1.3 Repeated Load on Concrete Members:

The brittle and quasi-brittle materials, like rocks and concrete, are widely utilized in engineering, mining, tunneling and the energy sector. Cyclic loading can cause severe damage or failure even when the load level is significantly less than the static short-term strength. 80% of all failure cases of engineering structures are caused by fatigue damage [6].

Concrete used for structures is subjected to numerous numbers of repeated loads during their service life. The performance of concrete to repeated load is usually determined by fatigue tests. most of these tests are administered mainly for determining the limitation of fatigue rupture of concrete, because structures become seriously dangerous when mechanical properties of concrete reach its fatigue limitation.

Since members of a structure are designed so that, the stresses that occurred in concrete stay beneath lower level of the failure limitation, it's therefore quite

seldom for concrete in actual structures to be subjected to such a higher-level repeated load which will end in fatigue rupture. However, repeated loads give concrete a gradual damage albeit the extent of stress is low, and it might cause reduction of durability of concrete [7].

1.4 Objective of the Thesis

This research aims to examine the structural behavior of non-prismatic reinforced concrete one-way slabs under the effects of repeated loads by experimental and numerical investigation. This would provide a basis for theoretical studies as well as engineering application of this type of slab.

The main objective of the present study can be summarized as follows:

1. Investigating experimentally the behavior of one-way prismatic and non-prismatic slabs.
2. Investigating the effect of providing one-way slabs with non-prismatic cross section on their bearing capacity and compare it with corresponding prismatic slab.
3. Finding the best configuration of tapered slab for different boundary condition.
4. Study the differences in the behavior of one way tapered one span, and continuous slabs.
5. A 3D finite element method using ABAQUS Standard/Explicit 2017 computer program was utilized for nonlinear analysis of reinforced concrete one-way slabs. Then, a comparison between the analytical and the experimental results was devoted for evaluating the validity and accuracy of using this analytical technique.

1.5 Layout of the Thesis

The thesis is divided into six chapters. This chapter gives some background on non-prismatic concrete members, also, it gives a description of repeated load on concrete members and briefly describes the structure of the thesis so that the reader can obtain a straightforward understanding of the content, and this thesis can be easily read.

In chapter two, review of the literatures from prior field research, which are related to the present study, is presented.

In order to understand the effect of providing non-prismatic cross section on the structural behavior of RC one-way slabs, eleven slab specimens are designed and tested as presented in chapter three. The details of the slab specimens, instrumentation, properties of the material, and the testing procedure used are carefully described, while the experimental results are presented and discussed in chapter four. The effect of each design parameter is studied separately.

Chapter five illustrates the finite element nonlinear analysis of the tested slabs, with a comparison between the finite element and the experimental results. After that, the effect of several different variables on the behavior of RC non prismatic one-way slab is studied.

Finally, Chapter six provides general and specific conclusions, together with suggestions for future research.

2

Chapter 2
Literature review

2.1 General

In this chapter, a brief review is carried out on the previous experimental and analytical studies on RC non-prismatic concrete members according to main studies in this field, also previous studies concerning prismatic and non-prismatic structural concrete members subjected to repeated load are presented. However, there was only one literature found related to non-prismatic concrete slabs.

2.2 Previous Studies on Non-Prismatic Concrete Beams

Tapered beams or hunched beams are the beams where the cross–section varies linearly along the length of the beam as shown in Figure 2-1. Tapered beams with negative hunch cross section have greater depth near the support, enough to resist the applied shear forces, and fewer depth at the middle, enough to resist the applied bending moment. The depth at the center may be increased if the applied load is high. While beams with positive hunch, have a cross section opposite of what was mentioned above.

Hunched beams have a wide range of application such as in framed buildings, cantilever retaining wall, simply supported and continuous bridges for economic and aesthetic purposes. Generally, the angle of the haunch or the angle of taper

varies from -12° to 12°. This restriction is due to construction complication and aesthetic view. [8]

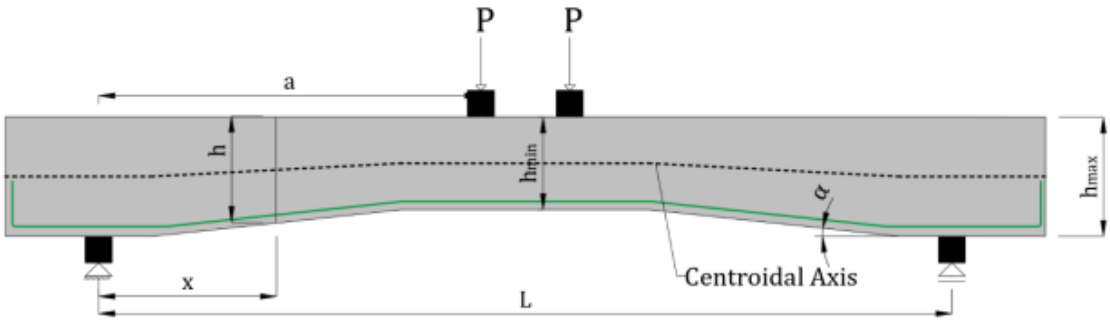

Figure 2-1: Negatively Hunched Beam [8]

Non-prismatic concrete beams or varied-depth concrete beams are utilized in buildings within the last decades. These beams are often used in various structures such as beam in mid-rise buildings, metro train pier cap and continuous bridges for aesthetic and economic reasons (see Figure 2-2). These sorts of structural members are supposed not only to be more economic, but also to resist load better than that of the prismatic beam. However, there is still little information about experimental data for predicting the shear behavior of non-prismatic reinforced concrete beams.[9]

Figure 2-2: Haunched capping beam [8]

This type of beams is also used for simply supported or continuous bridges as a lateral double cantilever hammerhead beam (see Figure 2-3).

Figure 2-3: Thawrat Al Eshreen Bridge in Iraq [10]

Actually, the planning of concrete hunched beams (RCHBs) has been left to judgment and knowledge of structural engineers in professional practice because the available codes and specific recommendations such ACI-318M-19 (American Concrete Institutes) or BS-5400 (British Standard Institutes) did not cover these sorts of members. Structural engineers and designers are often tending to use such non-prismatic beams due to the subsequent advantages with reference to prismatic beams:

a) Hunched beams substantially increase the lateral stiffness of buildings, which allows the designer to regulate code drift limits;

b) Such beams cause a more efficient use of concrete and steel reinforcement;

c) Reduce the load of structure for a given lateral stiffness;

d) the use of hunched beams facilitates the location of the air con, building's electrical and sewage equipment.[10]

Tan, (2004) [11] carried out a study on utilizing strut-and-tie models for the analysis and design of non-prismatic RC concrete beams. Seven beams were designed,

fabricated and tested to failure. Recess width, location, and strengthening scheme, were considered as major variables (see Figure 2-4).

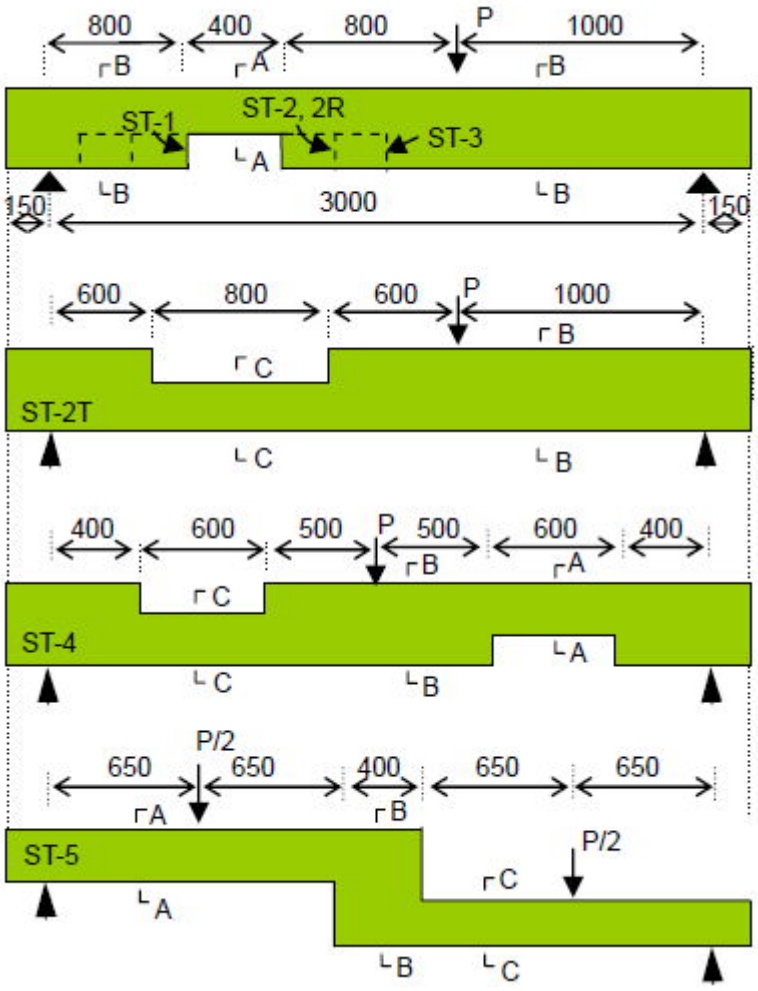

Figure 2-4: Dimensions of Kiang's Tested Beams (all dimensions in mm). [11]

The author compared the test results with design values and the following conclusions drowned from the above-mentioned study:

a) The strut-and-tie method of design was shown to be suitable for application in non- prismatic beams.

b) Non-prismatic beams with a recess exhibit comparable performance to beams with a transverse rectangular opening with reference to deflection and cracking characteristics, and supreme load behavior.

c) For non-prismatic beams with a recess within the tensile zone, a rise within the recess width leads to smaller ultimate load, higher cracking load and smaller service load deflection.

d) Beams with a recess introduced and subsequently strengthened with carbon FRP plates performed satisfactory with reference to strength, deflection and crack width. However, the failure tends to be non-ductile and sudden.

Archundia-Aranda et al., (2008) [12] tested ten simply supported reinforced concrete beams (eight haunched and two prismatic). These beams were designed to develop a shear failure under static loading. Five beams (four haunched and one prismatic) were tested without shear reinforcement whereas the remaining five (four haunched and one prismatic) were tested with a shear reinforcement satisfying the minimum required for prismatic beams by the concrete norms of Mexico's administrative district Code (MFDC).

The authors found that haunched beams have a special behavior with respect to prismatic beams. It was found that reinforced concrete haunched beams (RCHBs) develop an arch mechanism which allows the damage to be distributed in terms of several fissures along the haunched length before the main diagonal crack develops, then causing a failure mechanism that's less fragile than the standard sudden shear failure observed in prismatic beams, RCHBs indeed have more deformation capacity in shear than prismatic beams; however, they developed smaller ultimate shear strengths (Vu) with respect to the prismatic beams of reference.

Nghiep, (2011) [13] investigated the shear resistance of haunched concrete beams without shear reinforcement. His experimental program included tested 18 specimens. All test specimens were designed to possess an equivalent geometry for a bridge deck's slab in practice (see Figure 2-5). The results observed from the experimental program and nonlinear FEM analysis showed that, the inclination of haunched beams has a strong influence on the shear behavior as well as shear capacity of concrete beams without shear reinforcement

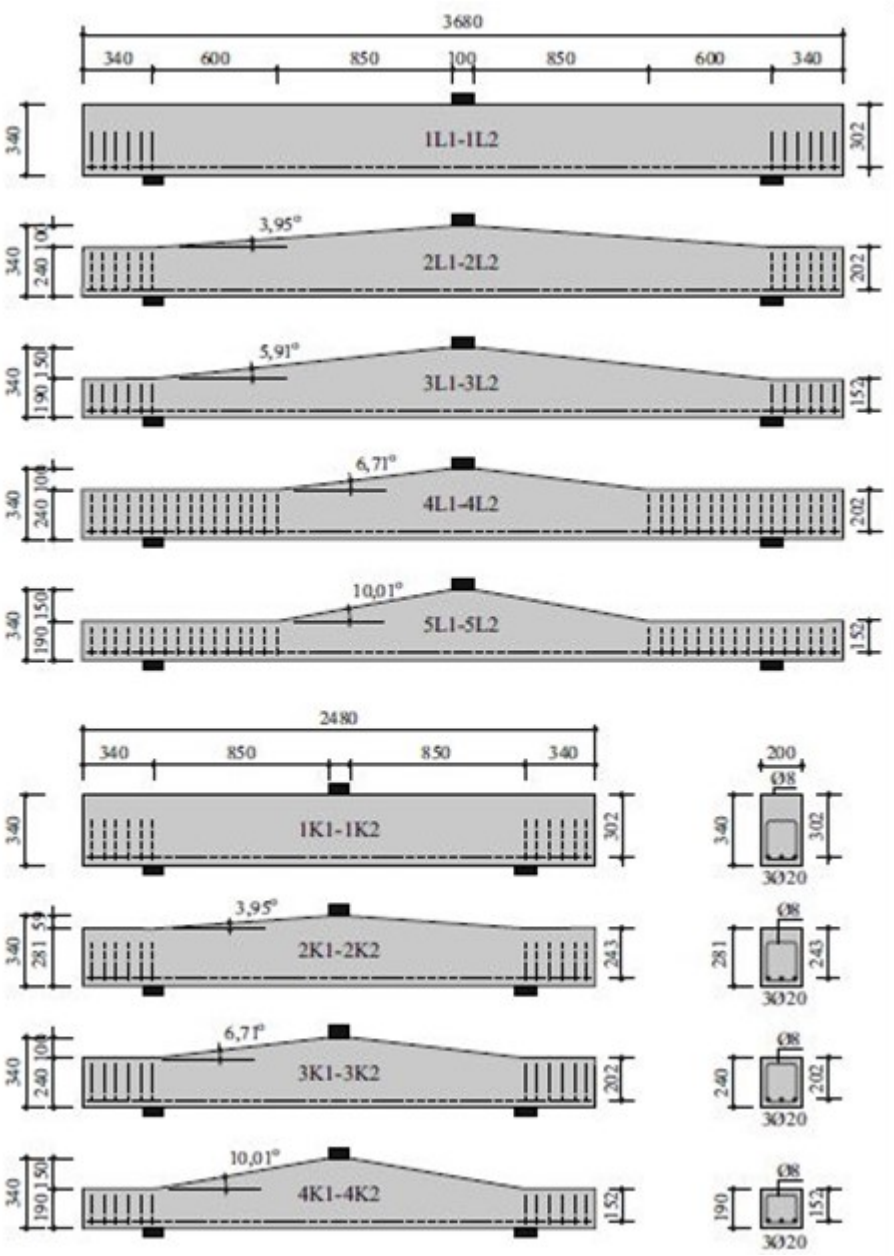

Figure 2-5: Geometrical dimensions of Hong's tested beams [13]

Nimnim. (2019) [14] divided specimens in his study into five groups following its five goals. the primary aim was to see the effect of compressive strength on the structural behavior of tapered and prismatic beams. The second aim was to review the effect of the tensile reinforcement ratio on the structural behavior of reactive powder concrete (RPC) tapered beams. The third aim was to review the influence of the tapering ratio on the structural behavior of RPC beams. The fourth aim was to review the influence of the shear reinforcement ratio. The last goal was to study

the effect of the tapering direction on the structural behavior of RPC beams. Therefore, nine simply supported beams were examined under one-point loading action at their midspans. Seven of the beams were tapered [six of them were made with RPC, and one among them was constructed with a normal concrete (NC)].

The last two beams had rectangular prismatic shapes (one of them was RPC, and the second was NC). All beams had the same overall length of 2,000 mm, a clear span distance equal to 1,850 mm, and the same width of 200 mm. The test results show that the tapered beam made with RPC had a superior ultimate load compared with the NC tapered beam and that the ultimate load increased when the tapering ratio increased. The ultimate load of the tapered beam was also found to be raised when the longitudinal and shear reinforcement ratio increased.

2.3 Non-Prismatic Concrete Beams Under Repeated or cyclic Loads:

Archundia-Aranda et al., (2013) [15] study how to confirm a ductile flexural failure of tapered beam. They tested ten prototype simply-supported reinforced concrete beams (eight haunched and two prismatic). These beams were designed to develop a shear failure under cyclic loading. Five beams (four haunched and one prismatic) were examined without shear reinforcement whereas the remaining five (four haunched and one prismatic) were examined with a shear reinforcement (see Figure 2-6).

These haunched beams are identical in geometry and reinforcement to a group of haunched beams previously tested under static loading. Authors doing these additional cyclic testing, taking under consideration parameters like the haunch angle, the concrete compressive strength, the shear reinforcement and in consequence the contribution of the inclined longitudinal reinforcement.

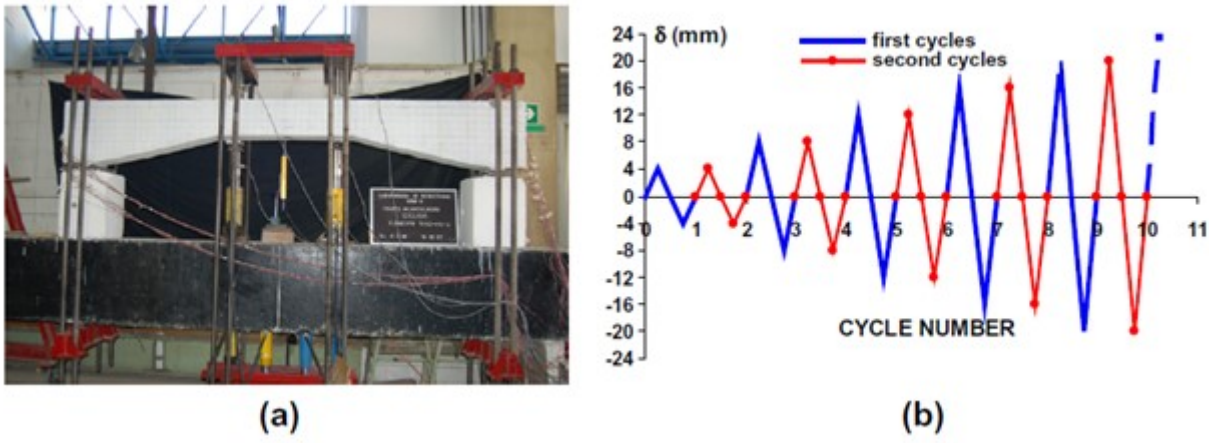

Figure 2-6: Experimental program: (a) testing setup and (b) cyclic displacement history [15].

From the obtained results, they found that haunched beams have a special cyclic shear behavior with reference to prismatic beams, having higher deformation and energy dissipation capacities, among other reasons, because non-prismatic beams favor an arching action within the haunched length because the main resisting mechanism, that develops smoother cracking patterns.

Dawood and Abdulkhaleq, (2017) [16] investigated the behavior of prismatic and non-prismatic continuous RC beams under influences of static and repeated loads. The experimental program made up of casting and testing fourteen specimens with different parameters. The studied parameters included the consequences of loading type (static and repeated load), concrete type (Reactive Powder Concrete and Normal Concrete), tapering ratio influence and existence of small circular openings with diameter 75 mm. All the specimens have an equivalent total length of 2440 mm with two spans, each span has clear distance adequate to 1150 mm.

The specimens were tested under effect of concentrated load in the mid of each span. The specimens were divided into four groups. The first group contains eight specimens to review the influence of loading type, four of them tested under influence of static load and the others under repeated loads.

The second group included four specimens to review the influence of concrete type on shear and flexural behavior of tested beams. The influence of tapering ratio was

studied with three specimens formed group three. The final group which examines the effect of small openings included four specimens.

Based on the results obtained from this study, the main conclusions were drawn: -

a) Experimental results explained that using RPC instead of NC in continuous beam enhanced the flexural ultimate capacity at about (51.22) % and recorded an increase in ultimate shear capacity more than (177.11) %, while the deflection decreases (65.93) % and (44.08) % for flexural and shear member respectively at the ultimate load of NC beams.

b) The RPC beams had a ductile behavior more than NC beams with percentage increment equal to (34.1) % and give an increase in total number of cracks (more warning before failure) at about (62.16) %.

c) Increasing tapering ratio from (1.33) to (1.594 and 1.875) with same amount of concrete enhanced from ultimate flexural capacity at about (7.56) % and (14.39) % and decreased the mid span deflection by (40.47) % and (34.35) % respectively at the ultimate load of control beam.

2.4 Previous Studies on Non-Prismatic Concrete slabs

Toshniwal, (2019) [17] in his study discusses different errors that engineers make in practice while performing cross-sectional analysis on non-prismatic bridge decks. The error in the cross-section results for different models are calculated for an existing bridge deck, Wolweg Bridge, The Wolweg Bridge is located near a village named Stroe, in the Gelderland province of The Netherlands

The bridge has 2 decks, with three spans per deck as shown in Figure 2-7. The length of the end decks is 10.5 m whereas the length of the middle deck is 13 m. Tapered section is provided near the intermediate support to increase the shear

capacity. The width of the deck is 20.8 m in the southern part, where the study is focused on.

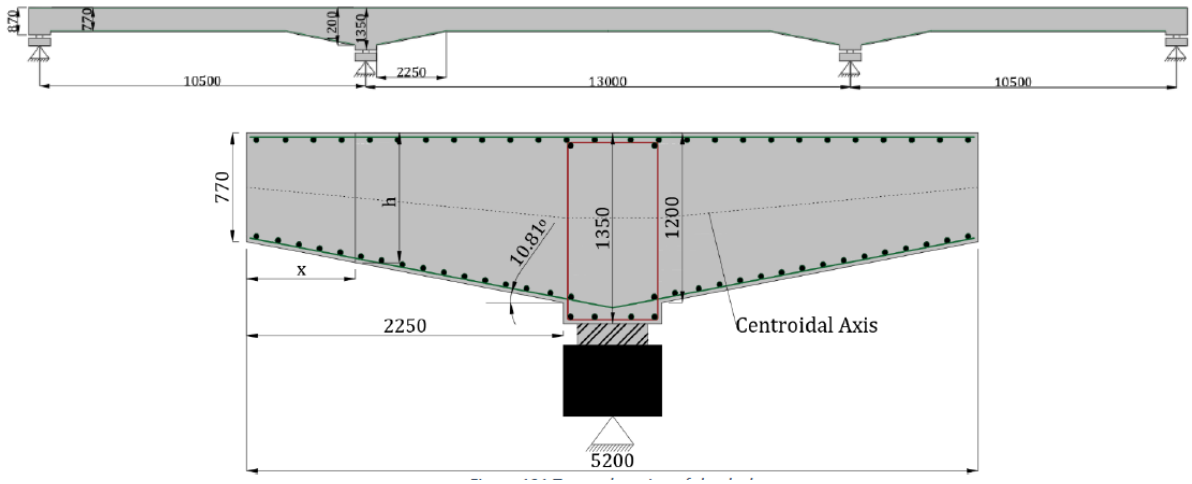

Figure 2-7: Deck dimensions and tapered section of the deck [17]

The height of the deck in the prismatic section is 770 mm whereas the maximum height in the tapered section is 1200 mm and that at the intermediate support is 1350 mm. The angle of taper is 10.81°. The length of the tapered zone is 2250 mm. In his study, Toshniwal focuses on the tapered section of the deck. Tapered section can be seen in Figure 2-8.

Figure 2-8: Tapered section at the intermediate support [17]

Toshniwal found that engineers make different errors while performing cross-sectional analysis of haunched concrete bridges, mainly because of the non-linear layout of centroidal axis. The haunched decks are modified by him such that the centroidal axis remains linear, with the same volume of concrete in use as shown in Figure (2-9). He found that this does not affect the shear capacity and bending moment resistance of the deck, but these results are obtained at Ultimate Limit State (ULS) and the structural behavior might differ in Serviceability Limit State (SLS).

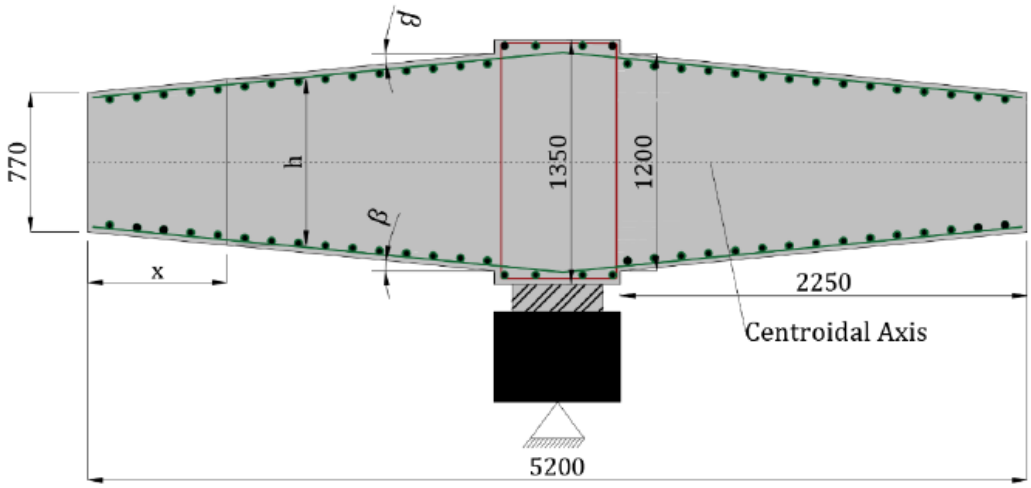

Figure 2-9: Modified tapered section of the deck [17]

2.5 Studied on Concrete Slabs under Repeated Loads:

Sivagamasundari and Kumaran, (2008) [18], carried out experimental studies on twenty-one number of one-way concrete slabs, (out of which three are reinforced with conventional steel reinforcements and eighteen are reinforced with Glass Fibre Reinforced Polymer (GFRP) reinforcements (see Figure 2-10).

A rigorous analytical and experimental studies on the behaviour of conventional and GFRP reinforced concrete one way slab under static and repeated loading were investigated by considering reinforcement ratios, grade of concrete, thickness of slab and type of GFRP reinforcements (with constant and variable amplitude loadings).

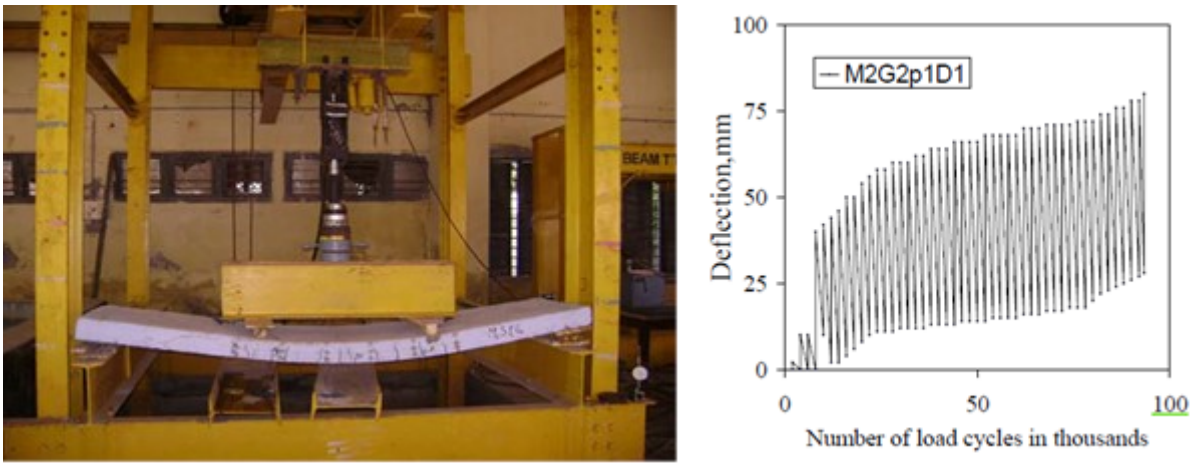

Figure 2-10: Testing setup and repeted displacement history [18]

All the slabs experienced flexural type of failure. At ultimate load, GFRP reinforced slabs experienced concrete crushing followed by the rupture of GFRP reinforcements. On increasing the thickness, grade of concrete, reinforcement ratio of the slabs, the ultimate load carrying capacities of GFRP reinforced slabs were increased and the corresponding strains in terms of deflection and crack width were reduced. GFRP reinforced concrete slabs experienced better performance and longer fatigue life when compared to the conventional slabs.

Al-Sulayvani and Diyar, (2015) [19] administered an experimental study to evaluate the effect of CFRP strips on the strengthening and repair of circular RC slabs with openings. Thirteen circular RC slabs with dimensions of (1200 mm in diameter and 75 mm in thickness) were tested under repeated loading through annular load subjected at the center of slabs. The slabs were simply supported on all edges. The experimental variables considered in this study include the shape of openings (circle, square, and rectangular) and the strengthening schemes (see Figure 2-11).

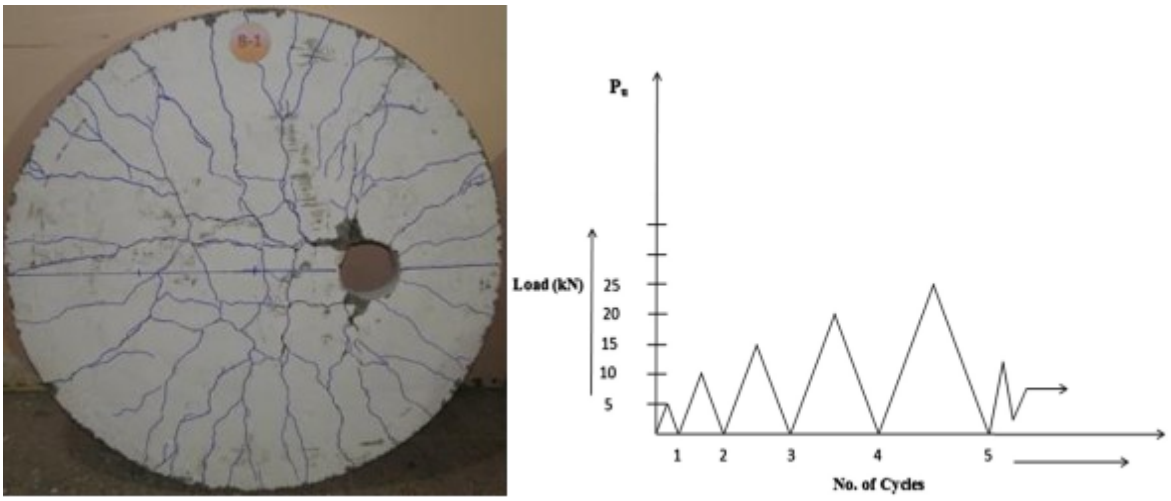

Figure 2-11: Cracks pattern at failure and the history of applied repeated loads [19]

The experimental results indicated that the use of CFRP strips to upgrade the circular RC slabs with openings has significant effect on ultimate load and deflection. Depending on the CFRP strengthening scheme used, the ultimate load capacity was increased by (27–52) %. The role of CFRP strips in repairing circular slabs was found to be bigger than its role in strengthening circular slabs.

Al-Shaarbaf et al., (2019) [20] made an experimental study to investigate the structural behavior of voided slab strips with normal and high strength Self Compacted Concrete (SCC) under repeated load. The experimental tests have been carried out on ten one-way simply supported slabs tested under monotonic and repeated loads. The fundamental conclusions drawn can be summarized as follows:

a) The flexural failure mode of specimens which were tested under repeated load was similar to that occurred in corresponding specimens tested under monotonic load.

b) Number of cracks occurred in slab specimens that tested under repeated loading scheme was larger than those took place in corresponding specimens which were tested beneath monotonic load.

c) The value of ultimate load of specimens tested under repeated loading system was smaller than that of corresponding slab specimen which was tested under

monotonic load. The ultimate load of specimens which have been tested under repeated load was decreased in range between 10% to 28.5% as compared with that of similar specimens tested under monotonic load.

d) The deflection at ultimate load of the specimens tested under repeated loading pattern was greater than that of corresponding specimens tested under monotonic load.

2.6 Summary and Concluding Remarks:

From the above review, it can be noticed that there are a few amounts of international and local researches that deal with one-way reinforced concrete slabs subjected to repeated loading. Also, only one research is found related to non-prismatic reinforced concrete slabs. Therefore, it still needs more information about the behavior of non-prismatic concrete slabs under repeated loads.

The present study implemented an analytical and an experimental investigation about the behavior of non-prismatic one-way slabs having different tapering configuration and different boundary conditions under repeated load.

3

Chapter 3
EXPERIMENTAL PROGRAM

3.1 Introduction

The main objective of the present work is to investigate the behavior of non-prismatic reinforced concrete one-way slabs under repeated load. Thus, an experimental investigation was carried out by testing eleven specimens of reinforced concrete one-way slab in the Structures Laboratories at University of Babylon.

The procedure of making, casting, and testing of the specimens are described. Furthermore, series of tests were conducted on several building construction materials, as well as control samples such as cubes, prisms, and cylinders to determine the concrete mechanical properties.

The properties of the materials used in the concrete have been verified to be according to the Iraqi specifications (IQ.S) and the American Society for Testing and Materials (ASTM).

3.2 Description of Specimens

Two groups of specimens were included in this study. The first group consists of one-way slabs with one span, while the second group included one-way slabs with

two spans. Slabs of both groups were designed according to ACI 318M-2019 [21] code (see Appendix A).

3.2.1 One spans one-way slabs (group 1)

This group consists of five slabs, three of them were simply supported, and the two remain slabs were fixed end supported. Slabs of this group were 1600 mm long, 500 mm wide, and with varying depths. All specimens were tested to failure under one-point loads at mid span, with 1300 mm clear span. It must be mentioned that, specimens of this group have the same total volume of concrete and reinforcement.

The three simply supported slab of this group were reinforced by 3 Ø 8 mm longitudinal steel reinforcement at bottom of each slab, also Ø 8 mm transverse steel reinforcement was provided each 200 mm at bottom of the short direction of each slab. The clear concrete cover was 20 mm. One of these slabs was prismatic with constant depth equals to 100 mm represents the reference slab of this group (S1 specimen). While, the two other slabs were non-prismatic with tapered cross section have varying depth. One of these two slabs was formed with positive haunch, the depth at mid span was 130 mm while it was 70 mm at supports (S2 specimen). The other slab has negative haunch with 70 mm depth at mid span and 130 mm at supports (S3 specimen).

For the two slabs with fixed end supported, the same amount of reinforcement that used in the bottom face of simply supported slabs was provided also at the top of these slabs due to presence of the negative moment at supports. One of them had the same dimensions as that of S3 specimen but with fixed end supports (S4 specimen). The last specimen of this group was fixed end support slab formed with double negative haunch with thickness (13 mm) at both center and support and (7 mm) at quarter span (S5 specimen). Figure 3-1 shows geometry, reinforcement, and tapered configuration for specimens of this group.

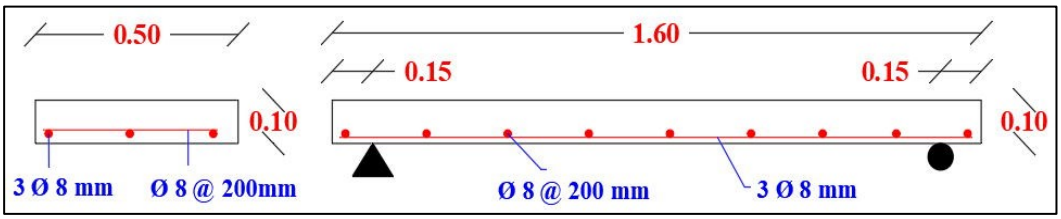

prismatic simply supported one span slab (S1 specimen)

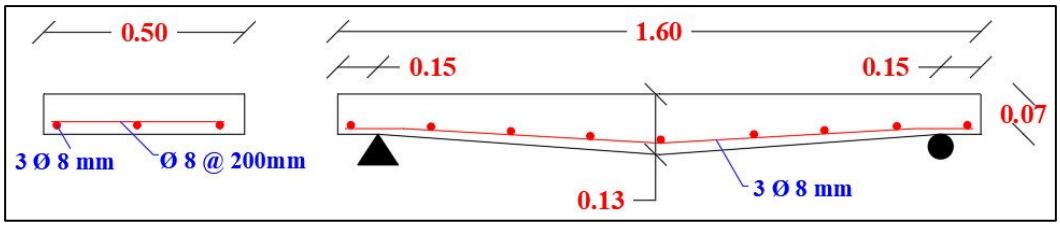

non-prismatic simply supported one span slab with positive haunch (S2 specimen)

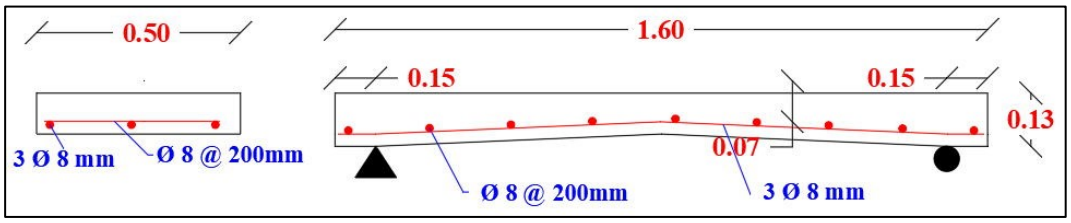

non-prismatic simply supported one span slab with negative haunch (S3 specimen)

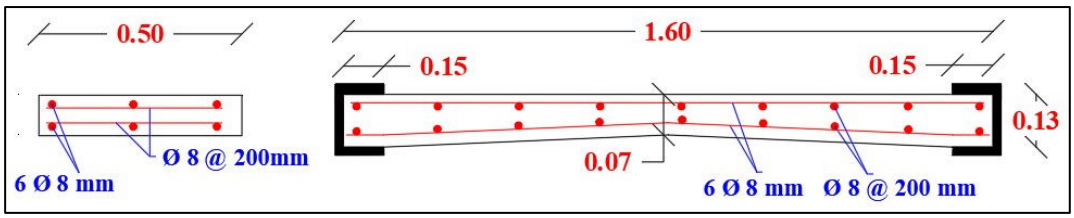

non-prismatic fixed end support one span slab with negative haunch (S4 specimen)

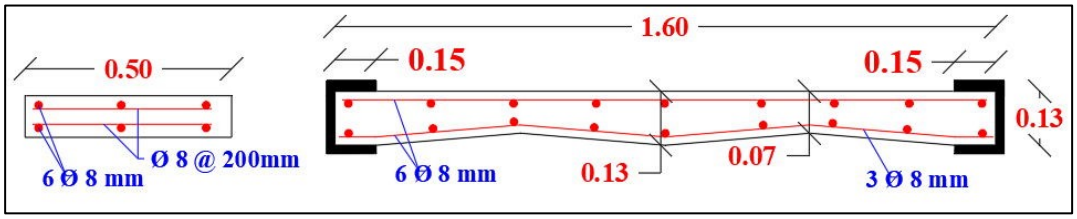

non-prismatic fixed end support one span slab with double negative haunch (S5 specimen)

Figure 3-1: Geometric and reinforcement details for one way slabs of the first group

3.2.1 Two spans one-way slabs (group 2)

Slabs of this group were 3000 mm long, 500 mm wide, and with varying depths. They comprised two equal spans of 1300 mm each. All specimens were tested to failure under two-point loads, one in the mid of each span. They were reinforced by

3 Ø 8 mm longitudinal steel reinforcement at top and bottom of each slab, also Ø 8 mm transverse steel reinforcement was provided each 200 mm at top and bottom of the short direction of each slab. The clear concrete cover was 20 mm.

This group consists of six slabs subdivided into two series based on the type of supports. The first series consists of three simply supported slabs. One of them were prismatic with constant depth equals to 100 mm represents the reference slab of this series (S6 specimen). While, the two other slabs were non-prismatic with tapered cross section have varying depth. One of these two slabs was formed with positive haunch, the depth at the center of each span was 130 mm while it was 70 mm at supports (S7 specimen). The other slab has negative haunch with 70 mm depth at mid span and 130 mm at supports (S8 specimen).

The second series consists of three slabs had the same dimensions and details as that of the first series specimen but with fixed end supports. Figures 3-2 and 3-3 show geometry, reinforcement, and tapered configuration for specimens of first and second series of this group respectively.

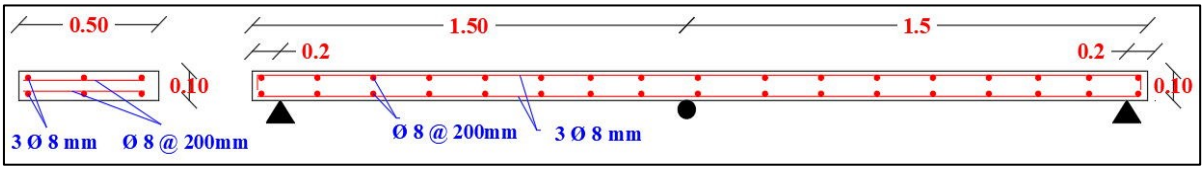

a) prismatic slab (S6 specimen)

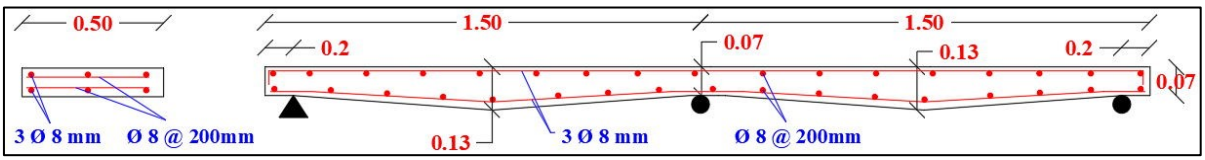

Non-prismatic slab with positive haunch (S7 specimen)

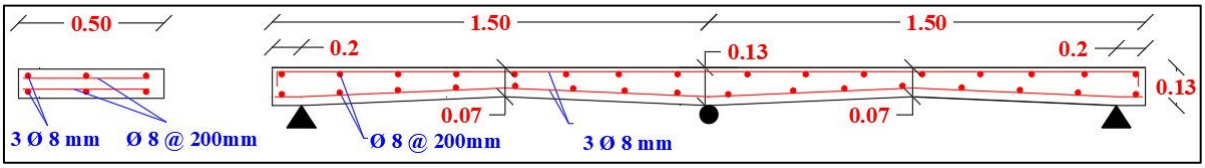

Non-prismatic slab with negative haunch (S8 specimen)

Figure 3-2: Geometric and reinforcement details for for simply supported two span slabs

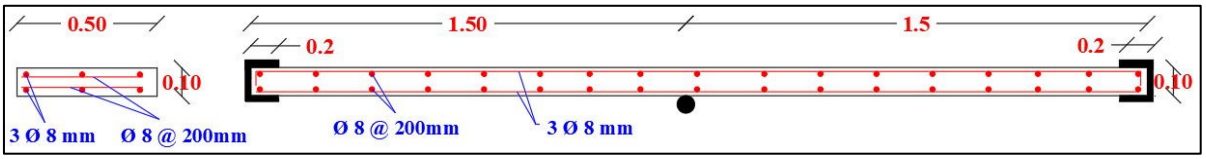

a) prismatic slab (S9 specimen)

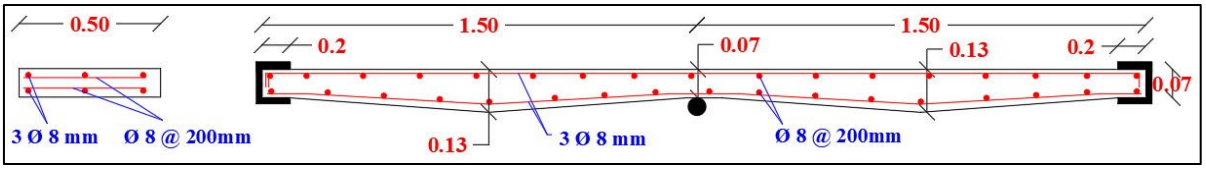

Non-prismatic slab with positive haunch (S10 specimen)

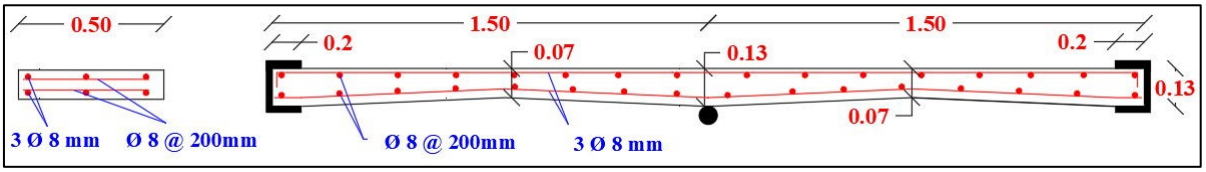

Non-prismatic slab with negative haunch (S11 specimen)

Figure 3-3: Geometric and reinforcement details for fixed end support two span slabs

3.3 Material Properties

3.3.1 Concrete

The materials used in producing concrete are locally available materials, which includes cement, natural gravel, natural sand, and water.

3.3.1.1 Cement

Ordinary Portland cement (Iraqi manufactured) named Karasta is used in this study for casting all specimens. Its chemical composition and physical properties as supplied by the manufacturer are given in Table 3-1 and Table 3-2, respectively, and it conforms to the Iraqi specification (IQ.S No. 5/1984) [22].

Table 3-1: Chemical analysis and main compounds of cement.

Chemical composition	*Item*	*Test Result (%)*	*Limits of Iraqi specification No.5/1984*
Silicon oxide	SiO_2	*20.58*	-
Aluminum oxide	Al_2O_3	*5.6*	-
Ferric oxide	Fe_2O_3	*3.28*	-
Calcium oxide	*CaO*	*62.79*	-
Magnesium oxide	*MgO*	*2.79*	≤ *5.0%*
Sulphur trioxide	SO_3	*2.35*	≤ *2.8%*
Loss of ignition	*L.O.I*	*1.94*	≤ *4.0%*
Insoluble residue	*I.R*	*1*	≤ *1.5%*
Lime saturation factor	*L.S.F*	*0.9*	*0.66-1.02*
Main compound composition			
Tri-calcium silicate	C_3S	*50.12*	-
Di-calcium silicate	C_2S	*21.26*	-
Tri-calcium aluminate	C_3A	*9.29*	-
Tetra-calcium aluminate ferrite	C_4AF	*9.98*	-

Table 3-2: Physical properties of cement.

Item	*Test Result*	*Iraqi specification No. 5/1984*
Blaine fineness (m2/kg)	*314*	≥ *230*
Compressive Strength (MPa) *3 days* *7 days*	 *20.8* *28.0*	 ≥ *20* ≥ *23*
Time of setting (Vicat) *Initial (hours: minutes)* *Final (hours: minutes)*	 *2:05* *4:20*	 ≥ *00:45* ≤ *10:00 hrs*

3.3.1.2 Fine Aggregate (Sand)

Natural sand of 4.75 mm maximum size is used in this investigation. Table 3-3 shows grading and properties of fine aggregate, which conforms to the Iraqi standard specification (IQ.S No.45/1984) [23].

Table 3-3: Fine aggregate grading and properties*

Sieve's opening size	*passing %*	
	Fine aggregate	*Iraqi specification No. 45/1984 Zone (2)*
10 mm	*100*	*100*
4.75 mm	*92*	*90-100*
2.36 mm	*81*	*75-100*
1.18 mm	*73*	*55-90*
600 μm	*55*	*35-59*
300 μm	*24*	*8-30*
150 μm	*7*	*0-10*
SO3 content=0.35% (specification requirements up to 0.5%) *Fineness modulus = 2.68*		

* Test was conducted in the construction material laboratory at University of Babylon

3.3.1.3 Coarse Aggregate (Gravel)

A maximum size of 14 mm of local gravel is used in the current study. The gravel was washed and cleaned by water several times and left to dry in air. Table 3-4 shows grading and properties of the coarse aggregate, which conforms to the Iraqi standard specification (IQ.S No.45/1984) [23].

Table 3-4: Coarse aggregate grading and properties*

Sieve size (mm)	*Passing %*	
	Coarse aggregate	*Iraqi specification No.45/1984*
19	*100*	*100*
14	*96*	*95-100*
10	*46.6*	*8-50*
5	*5.1*	*0-10*
2.36	*0.2*	*-------*
SO3 content=0.07% (specification requirements up to 0.1%)		

* Test was conducted in the construction material laboratory at University of Babylon

3.3.1.4 Chemical Admixtures

Sika ViscoCrete® 5930-L (Figure 3-4) that is a third-generation high range water reducing admixture (HRWRA), was used in producing the concrete. It was used with a nominal dosage of (0.8 - 2 % liter by weight of cement) as recommended by the manufacturer. Sika ViscoCrete® 5930-L meets the requirements for SP in according with ASTM C494 / C494M – 17 standard [24]. The manufacturer's datasheet of this products is presented in Appendix B.

Figure 3-4: SikaViscocrete-5930

3.3.1.5 Mixing Water

Tap water has been used for casting and curing all the slab specimens.

3.3.2 Reinforcing Steel Bars

Deformed hot rolled mild steel bars (BRC Turkish production) of 8 mm in diameter were used as reinforcement in all reinforced concrete slabs. The tensile test (for three specimens of steel bars) was done at the materials laboratory of the engineering of materials college at the University of Babylon following ASTM A1064 / A1064M - 18a standard test [25]. The digital machine used for testing steel bars is shown in Figure 3-5 and the results are presented in Table 3-5.

Table 3-5: Test results of steel reinforcing bars.

Nominal diameter (mm)	*Measured diameter (mm)*	*Density (kg/m3)*	*Yield stress (MPa)*	*Tensile strength (MPa)*	*Elongation %*
8	*7.9*	*7844*	*550*	*678*	*7*

Figure 3-5: Digital machine used for steel bar testing

3.4 Mix Design

In order to select the mixture proportion for normal weight concrete with target compressive strength of 37 MPa at 28 days. The adopted mix was made utilizing the mixture proportion that used by Oday M. A., 2013. The selected mixture for casting all slab specimens was (1 cement: 1.7 sand: 2.3 gravel, by weight). It was found that the used mixture produces good workability and uniform mixing of concrete without segregation. The average compressive strength f_{cu} at 28 days was 46 MPa. Table 3-6 shows the mixture proportions (by weight) of the selected concrete mix.

Table 3-6: Mixture proportions for the selected concrete mix.

Materials	*The selected concrete mix*
Water/cement ratio	*0.3*
Superplasticizer Sika ViscoCrete® 5930-L (Liter)	*4.5*
Cement (kg/m³)	*450*
Fine aggregate (kg/m³)	*765*
Coarse aggregate (kg/m³)	*1035*

3.5 Specimens Preparation

This part includes reinforcement cages and mold preparation, mixing procedure, casting and curing of the specimens.

3.5.1 Reinforcement Cages and Mold Preparation

Deformed steel reinforcement bars with 8 mm diameter were used to manufacture the reinforcement cages for all slab specimens. The steel bars were cut and bent to desired dimensions. The steel bars were tied together using bending steel wires to form the steel cages. Figure 3-6 shows manufacturing cage of steel reinforcement used in the experimental work.

Figure 3-6: Manufacturing cage of steel reinforcement

Plywood molds were prepared to accommodate the reinforcement cages. The mold consists of five separate parts that can be collected in an easy way, it designed to be easy in collection or taking apart without any effect in the casted specimen. Before casting, this form works was oiled and put in horizontal levels. After completing the preparation of the mold, the reinforcement cages held carefully to their position inside the mold. In order to get the cover, small pieces of plastic spacers were used to allocate the reinforcement cage at the correct bottom and side distance from the molds. Figure 3-7 shows the appearance of the mold with the reinforcement cage inside and ready for casting.

Figure 3-7: Reinforcement cages in molds prior to casting.

3.5.2 Mixing, Casting, and Curing

One batches of concrete are used to cast all slabs at the same day. The concrete was prepared and delivered by a local ready-mix concrete producer. Mixing of concrete was performed with according to ASTM C192-07 [26]. All slabs were casted together with, six-cylinder specimens of 150 mm diameter and 300 mm height, six (150×150×150) mm cubes, and seven (100×100×400) mm prisms to determine the concrete mechanical properties. The concrete was poured into the lightly oiled mold in two layers and well compacted by plunger mechanical vibrator (3500 rpm), 5

seconds for each insertion. The surface of the concrete was levelled off and finished with a steel trowel. Figure 3-8 shows the casting stages of the specimens.

Figure 3-8: Casting stages of the beam specimens

All specimens were demolded after 24 hours of the casting, then burlap sacks were placed over the slabs and kept wet until 28 days. Cylinders, cubes, and prisms were placed in curing water tank and kept wet in accordance with the standard specifications. After (28) days, they were taken out of the curing basin and then tested. On the other hand, the concrete surfaces of the slab specimens were painted white, and prepared for testing; see Figure 3-9.

Figure 3-9: Demolding, curing, and painting the slab specimens

3.6 Instrumentation

The instrumentation of the slab specimens was designed to register the maximum quantity and most reliable data of deflections, and crack widths.

- In order to measure the deflection of the tested one span slabs, two vertical digital dial gauges were used, one at the mid-span section, and the other vertical dial gauge was placed at one of the slab quarters in the longitudinal direction. For slabs with two span another dial gauge was used under the center of span two. All dial gauges were attached to vertical metallic elements and fixed in vertical position during the test. These dial gauges have a maximum measurement of 30 mm and accuracy of 0.01 mm; see Figure 3-10.

Figure 3-10: Mechanical dial gauges used in this study

- An optical micrometre with an accuracy of 0.02 mm was used to measure crack width for all beam specimens; see Figure 3-11.

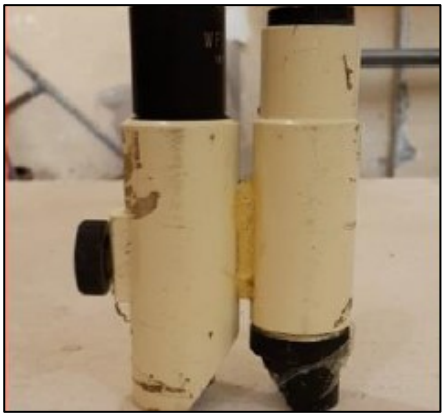

Figure 3-11: Optical micrometer to measure crack width

- In addition to the above, two types of support were used in this study. Smooth rod and bearing plate were used to represent the simply support. While for fixed support, two holes on each side of slab were made with a drill device and then screws were used to join two steel blocks together so that it is held tightly in place and fixing the sample ends on the test device girder as shown in the Figure 3-12.

Figure 3-12: Preparing stages of fixed supported in this study

3.7 Test Setup and Procedure

Eleven concrete slabs were tested under repeated loads until failure by using 600 kN capacity hydraulic testing machine at Structural Laboratory of the Civil Engineering Department of Babylon University. Each slab was placed with its

specific supports. For one span slabs one line load was applied at the center of slab. While for two span slabs, two-line loads were applied to the tested slab through a spreader steel beam. Bearing plates were used at supports and loading points to avoid local crushing in concrete. Webcam cameras were used during the test to record the load and dial gauges reading at the same time by connected them to a computer. Figure 3-13 shows the details of the machine used in the test.

Figure 3-13: The universal testing machine and test configuration.

At the beginning, the dial gauges were set and checked by applying 2 kN as an initial load. Then, the load was returned to zero. After that (at zero loadings), the initial reading of dial gauges was recorded. The load was applied from zero to the ultimate load by several stages. The applied load at each stage was increased by 20% of the designed ultimate load for each slab. Thus, the first stage was started from zero to 20% of the designed ultimate load and then to zero and repeat this load process five times. The second stage was up to 40% of the designed ultimate load. The next stage was up to 60% of the designed ultimate load. The fourth stage was up to 80% and so on until failure, each stage was repeated five times (see Figure 3-14).

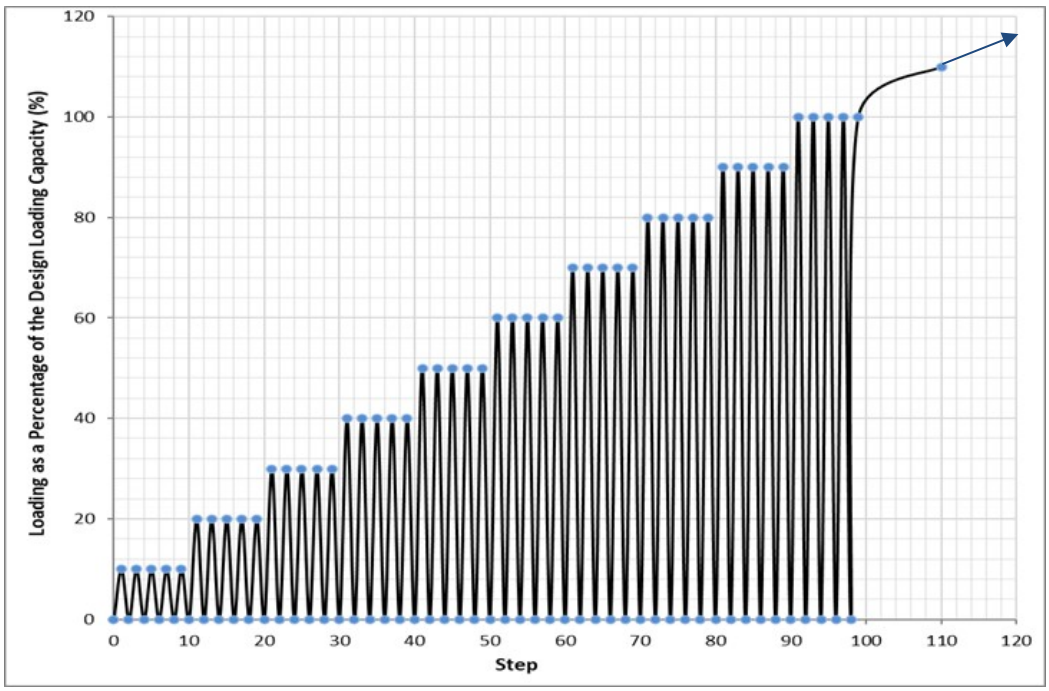

Figure 3-14: Loading Protocol

At each loading increment, crack width was measured using a crack meter (Figure 3-15), and deflection was recorded using dial gauges. Additionally, the location of the first crack and the magnitude of the first cracking load were recorded. Cracks development on each model were also traced and outlined by a permanent marker.

Figure 3-15: Recording crack width

3.8 Mechanical Properties of Hardened Concrete

3.8.1 Compressive Strength

Concrete compressive strength of cubes and cylinders was obtained according to BS1881-part 116:1989 [27] for cubes and ASTM C39/C39M – 20 [28] for cylinders. The tests were carried out at the structural laboratories of Babylon University. Three cubes of (150×150×150) mm and three cylinders of (150×300) mm were tested at 28 days by using automatic compression testing machine with 2000 kN capacity, the load was applied at rate of 0.3 MPa per second. Figure 3-16 shows the compressive strength test setup.

(a) Cube compressive strength test

(b) Cylinder compressive strength test

Figure 3-16: Compressive strength test setup

3.8.2 Tensile Strength

Different definitions for the tensile strength can be distinguished: the axial tensile strength (the tensile strength of a specimen subjected to an axial stress), the flexural tensile strength (that of a specimen subjected to a flexural stress) or the splitting tensile strength.

In this work, the concrete tensile strength was determined at the structural laboratories of Babylon University by splitting tensile tests on cylindrical specimens and the flexural tensile strength of prismatic specimens (modulus of rupture).

Concrete prisms specimens of dimensions (100×100×400) mm were tested with third-point loading according to ASTM C78-2010 [29]. All prisms were tested at 28 days by using a universal flexural testing machine with a capacity of 150 kN, the rate of load was 1 MPa per minute. Figure 3-17 shows the modulus of rupture test setup.

Figure 3-17: Concrete flexural tensile test setup

The splitting tensile strength was carried out on cylindrical concrete specimens of 150 mm diameter and 300 mm height in accordance with ASTM C496-2011 [30]. The specimens were tested at 28 days by using automatic

compression testers for cubes and cylinders with a capacity of 2000 kN, the rate of load was 0.018 MPa per second. Figure 3-18 shows the splitting tensile test setup.

Figure 3-18: Concrete splitting tensile test setup

4

Chapter 4
EXPERIMENTAL RESULTS AND DISCUSSION

4.1 Introduction

In this chapter, the most relevant results obtained from experimental program that described in chapter three are summarized and discussed.

First, the properties of hardened concrete obtained from tests of the control samples (cubes, cylinders, and prisms) as shown in the last section of chapter three are displayed. Then, test results obtained from specimens are represented and discussed including, ultimate load, modes of failure, load-deflection response, and results of cracking behaviour and ductility are also attained.

It must be mentioned that in this study, the effects of three parameters on the overall behavior of slabs were studied, including:

1- The influence of tapering configuration on the behavior of non-prismatic slabs under repeated load.

2- Behavior of slabs with different type of ending supports under repeated load.

3- Behavior of slabs with different number of spans under repeated load.

4.2 Mechanical properties of concrete

After duration of curing (28 days), several tests were carried out on the control samples (cubes, cylinders, and prisms) to find the mechanical properties of the hardened concrete, which used to cast all the specimens. the average of three samples has been taken to calculate each value, the results are shown in Table 4-1.

Table 4-1: Mechanical properties of the hardened concrete.

Cube Compressive Strength f_{cu} (MPa)	*Cylinder Compressive Strength f_c' (MPa)*	*Splitting Tensile Strength f_{sp} (MPa)*	*flexural tensile Strength f_r (MPa)*
46.92	*35.2*	*3.28*	*4.69*

4.3 Test results of specimens

As mentioned before two groups of specimens are tested to study the behavior of non-prismatic reinforced concrete one-way slabs under repeated load. Results are compared to investigate the significance and effect of experimental variables, which include tapering configuration, type of ending supports and number of spans.

4.3.1 Test Results of One Span RC One Way Slabs (Group 1)

The following sections discuss the outcomes of the experimental study using characteristics including ultimate loading capacity, load-central deflection curves, the load of the first crack, the deflection and the crack width corresponding to the service load, crack pattern and failure mode, deflection ductility and energy absorption index for one span RC one-way slabs (group 1).

4.3.1.1 Load – Deflection Response and Ultimate Loads

A vertical dial gauge placed at the mid-span position registers the mid-span deflection. Figure 4-1 shows the load-midspan deflection behaviours for all tested slabs of this group. Generally, the typical load-deflection curve can be divided into three stages: pre-cracking, post-cracking, and ultimate stage.

At early loading stages, all slab models were in the elastic-untracked state (elastic stage) that starts from zero-loading until cracks developed. In this stage, the deflection increased in all slab specimens linearly as the loading increased.

The second stage was the elastic-cracked (the elastic-plastic stage) that started after cracks initiation until yielding of the longitudinal reinforcement was developed. In this stage, almost a linear correlation was observed between the applied load and the corresponding deflection but with different slopes.

The third stage was the ultimate stage (the plastic stage) that started after yielding of the longitudinal reinforcement. In this stage, a non-linear relationship was developed in the load-deflection curves with a reduction in the slope of the curve and rapid increase in the deflection up to failure of the tested concrete slab.

As shown in Figure 4-1a, the load-deflection curve for non-prismatic slab with positive haunch (S2 specimen) is stiffer than the prismatic one (S1 specimen). This behaviour is due to the increase in the cross-sectional area at the critical section (mid span) and that enhanced the flexural rigidity and internal moment capacity, and vice versa for negative haunch slab (S3 specimen) which show larger deflections relative to reference slab at the same load stage.

With regard to the support condition, Figure 4-1b shows that slab with end fixed support is stiffer than simply supported slab despite the reduction in the cross-sectional area at the critical section due to the decrease in the slab thickness from 10 mm to 7 mm for negative haunch slab (S4 specimen). However, for fixed end one-way slabs the load-deflection response for double negative haunch slab with 13 mm thickness at center (S5 specimen) is stiffer than negative haunch slab with 7 mm thickness at center (S4 specimen).

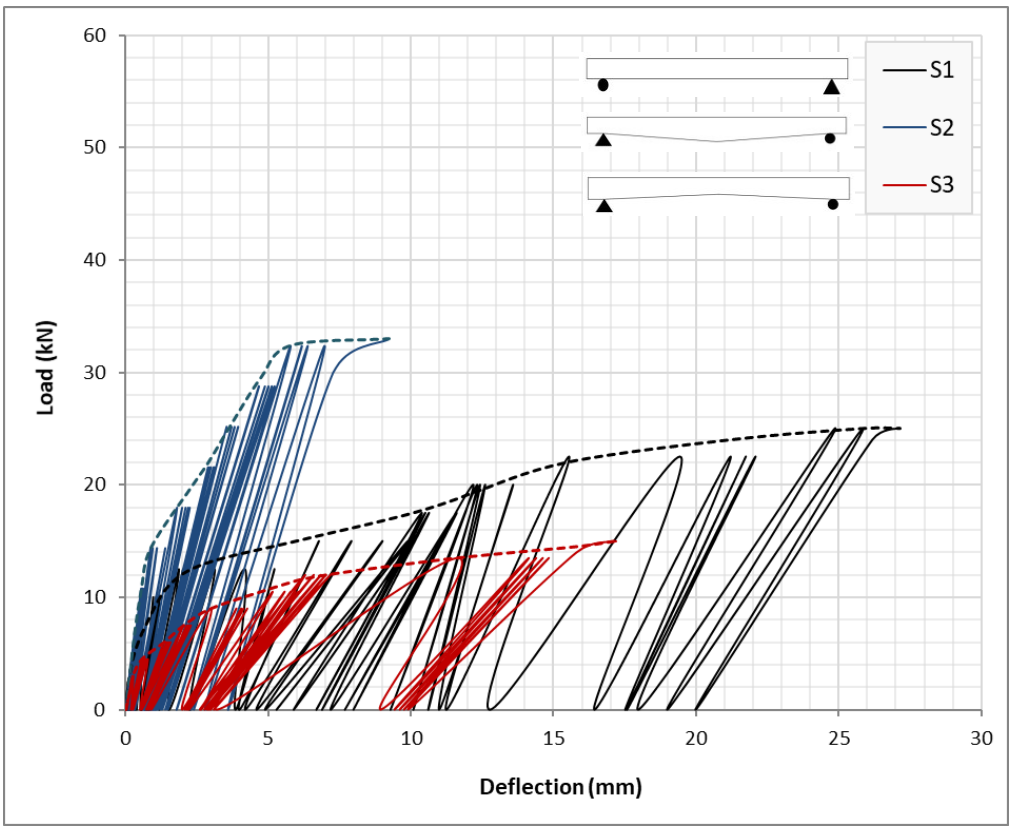

(a) Effect of tapering configuration

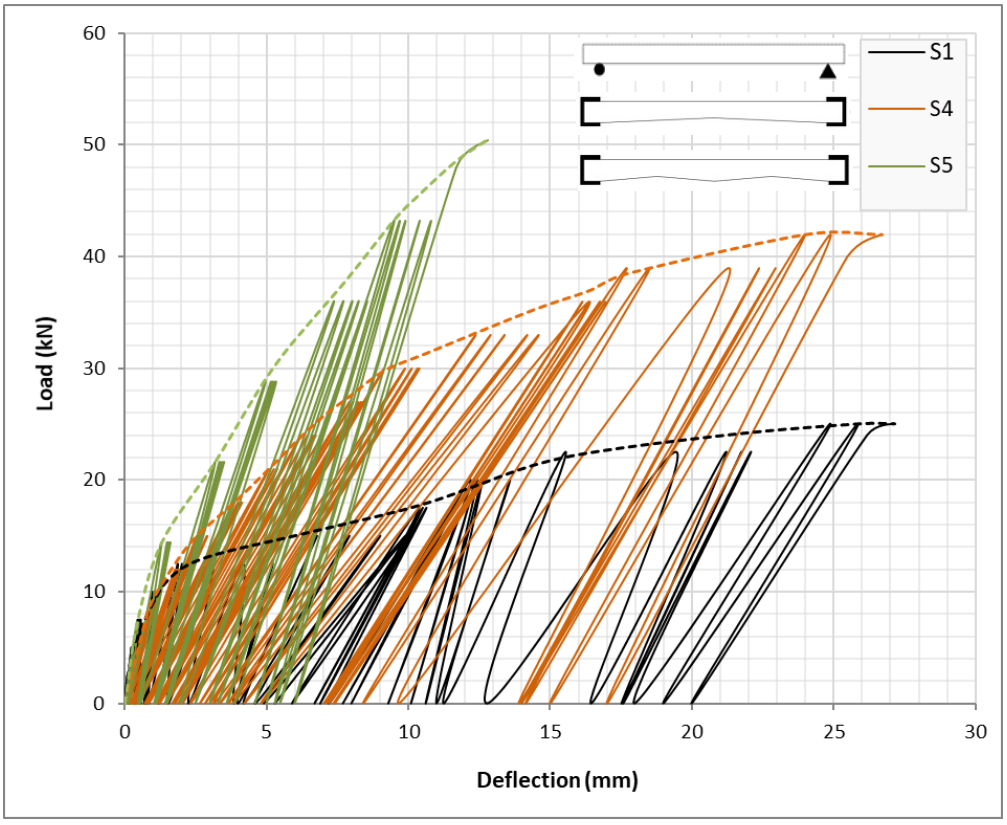

(b) Effect of the support condition

Figure 4-1: Experimental Load - Midspan deflection curves for one span slabs.

During the loading-unloading process, the path of the ascending part of the load-deflection curve was not the same as the descending part; the difference between the two paths is usually called the Dissipated Energy. The experimental test results showed that there is an increase in deflection at the same point and the same increment of the load with an increase number of cycles of loading for all the specimens. That causes slab not to return to the original position when the load decreased to zero level at the end of each cycle of loading.

The ultimate load capacity (Pu), the mid span deflection at service load, and the mid span deflection at ultimate loads for one span slabs are presented in Table 4-2. The deflection at the service load level is compared with the limitations of ACI 318-19 for immediate deflection for floors due to maximum live load (Lc/360 = 3.61 mm) [21]. It is observed that the load capacity of slab increases by 32% when using positive haunch (S2 specimen). While for negative haunch (S3 specimen), the reduction in the load capacity is 40% from the ultimate load of the prismatic slab. That attributed to the reduction in the concrete depth at critical section which effect the internal moment capacity.

With regard to the support condition, it is found that using fixed at both end in S4 and S5 specimens have a significant effect on increasing the ultimate load capacity compared to simply support slab. On the other hand, providing positive haunch caused decrease in the deflection at both service and ultimate load compared to prismatic slab.

Table 4-2: Ultimate load capacity and deflection at mid span for one span slabs.

Specimens designation	*Ultimate load Pu (kN)*	*Deflection at service load* , δs (mm)*	*Deflection at ultimate load, δu (mm)*
S1	*25*	*6 ***	*27.15*
S2	*33*	*2.3*	*9.24*
S3	*15*	*3*	*17.19*
S4	*42*	*6.75 ***	*26.7*
S5	*50.4*	*5.3 ***	*12.8*

* Assumed service load = 60% from ultimate load of each slab

** Did not satisfy the limitations of ACI 318-19 [21] for immediate floors deflection which is 3.61 mm

4.3.1.2 Cracking Behavior and Modes of Failure

At the early stages of loading, reinforced concrete slabs are free from structural cracks, with increasing the load and when the stresses exceed the tensile strength of the concrete, cracks will progress from the tensile portion of the cross-section. The first crack was a vertical flexural crack in the maximum bending zone (at mid span), its growths slowly across the width of the slab (i.e., parallel to the supports). After that, flexural cracks developed and formed parallel to that crack and slowly propagated throughout the thickness of the slab. As the load increases, some cracks that were vertical near the supports start to incline toward the concentrated load due to the combined effect of flexural and shear, it is referred to as flexural-shear cracks. Finally, no more cracks appear and the existing ones widen. However, for non-prismatic slab with negative haunch, cracks were concentrated at the middle third. This is attributed to the smaller thickness in this portion. While for slab with positive haunch flexural-shear cracks were appear near supports (see Figure 4-2).

a) Positive haunch (S2 specimen)

a) Negative haunch (S3 specimen)

Figure 4-2: Crack pattren after failure for non-prismatic one span slabs

A further increase in the load magnitude or the number of cycles of the repeated load led to more reduction in the stiffness of the slab models (plastic stage) then after the rapidly increased in the deflection and width of some cracks at mid-span section, RC slabs of this group failed by yielding of the main reinforcement bars followed by concrete crushing. The concrete crushing took place in the central zone at the top of the slab. This mode of failure was obtained for all one span slabs except for the fixed end support slab with thickness (13 mm) at both center and support and (7 mm) at quarter span (S5 specimen), which failed by shear. The shear failure for this specimen was brittle and without warning. This mode of failure occurred here as a result of reduction in the slab thickness which effect the required concrete area for shear strength in the quarter span. Observations of cracks development were marked along the whole length of the slabs at the different load steps. Figures (4-3) to (4-7) shows the cracks pattern and failure modes obtained for slab of this group.

Figure 4-3: Cracks pattern at failure for prismatic simply supported one span slab (S1 specimen)

Figure 4-4: Cracks pattern at failure for non-prismatic simply supported one span slab with positive haunch (S2 specimen)

Figure 4-5: Cracks pattern at failure for non-prismatic simply supported one span slab with negative haunch (S3 specimen)

Figure 4-6: Cracks pattern at failure for non-prismatic fixed end support one span slab with negative haunch (S4 specimen)

Figure 4-7: Cracks pattern at failure for non-prismatic fixed end support one span slab with double negative haunch (S5 specimen)

The experimental first cracking load (Pcr), width of first crack and mode of failure for each tested slabs of this group are presented in Table 4-3.

Table 4-3: Experimental first cracking load and width with failure mode for one span slabs.

Specimens designation	*First cracking load (kN)*	*Deviation in cracking load (%)*	*Crack width at servic load for the first crack (mm)**	*Modes of failure*
S1	*9.2*	*-------*	*0.22*	*flexural*
S2	*14*	*52.174*	*0.08*	*flexural*
S3	*4.5*	*- 51.08*	*0.32*	*flexural*
S4	*5*	*- 47.36*	*0.8 **	*flexural*
S5	*10.5*	*10.5*	*0.36*	*flexural-shear*

* Assumed service load = 60% from ultimate load of each slab
** Did not satisfy the limitations of ACI 318-19 [21] for maximum crack width which is 0.4 mm.

It is observed that the reduction in the first cracking load for non-prismatic slab with negative haunch is 51.08% with respect to the reference slab. While, non-prismatic slab with positive haunch shows a significant increment in the first cracking load. This is attributed to the change in the concrete depth at critical section which effect the moment of inertia. Thus, increase in slab depth caused increase in moment of inertia then increasing the required load for develop the first crack.

The experimental first crack width was measured by an optical micrometre at cracking and service load as shown in Table 4-3. It is found that, the width of the first crack at the first cracking load is approximately 0.02 mm and it is the same for all specimens. In general, providing cross section with negative haunch caused an increase in the width of the first crack at service load and that did not satisfy the limitations of ACI 318-19.

4.3.1.3 Ductility

Ductility for a structural member could be defined as the capability of the member to experience significant deflection before failure. This property is essential for structural members subjected to seismic loads since it provides signs of failure

beyond yielding and before failure. Two ductility definitions were explored here: Deflection ductility index (μd), and Energy absorption index (EAI).

Deflection ductility index defined as the ratio of the deflection at ultimate load of the slab to the deflection at yielding of the longitudinal tensile reinforcement, while the energy absorption index defined as the ratio between the total area under the load-deflection curve to that under the elastic part only (up to the yielding point). Therefore, identifying the yielding point of a load-deflection curve is essential [31]. Various approaches to estimate the yielding displacement are available in the literature. In this research, an approach that previously proposed by Priestley and Park, 1987 [32] is adopted. In this approach, (δy) is the yield displacement of the equivalent elasto-plastic system with reduced stiffness found as the secant stiffness at 75% of the ultimate load of the real system, as demonstrated in Figure (4-8). This methodology can be expressed by equations, Eq. (4-2) for deflection ductility index and Eq. (4-3) for energy absorption index.

$$\text{Deflection ductility index, } \mu d = \frac{\delta u}{\delta y} \quad \text{----------(4-2)}$$

$$\text{Energy absorption index, } EAI = \frac{A1+A2}{A1} \quad \text{----------(4-3)}$$

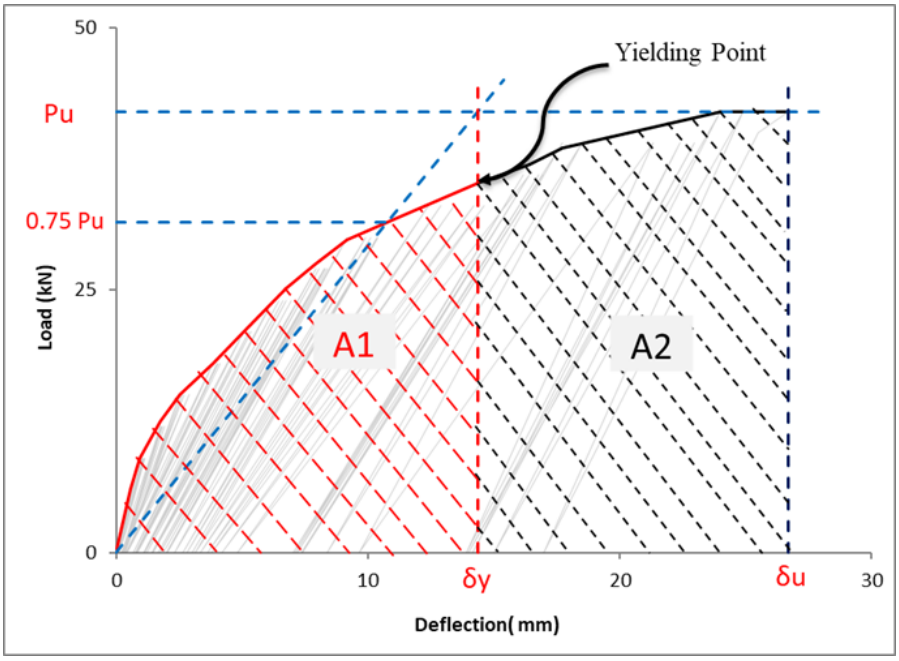

Figure 4-8: Typical diagram for determining the ductility index of RC slabs (S4 specimen).

The results of deflection ductility index and energy absorption index with all the parameters that required to determined them for slabs of this group are presented in Table 4-4.

Table 4-4: Ductility index for one span slabs.

Beam designation	*Yield deflection δy (mm)*	*Deflection at Ultimate load δu (mm)*	*Deflection ductility index μd*	*Elastic area A1 (kN.mm)*	*Plastic area A2 (kN.mm)*	*Total area A1+A2 (kN.mm)*	*Energy absorption index EAI*
S1	*15.5*	*27.15*	*1.75*	*244*	*277*	*521*	*2.135*
S2	*4.73*	*9.24*	*1.95*	*91*	*146*	*237*	*2.6*
S3	*7.6*	*17.19*	*2.26*	*68*	*130.6*	*198.6*	*2.92*
S4	*14.35*	*26.7*	*1.86*	*343.5*	*490*	*833.5*	*2.42*
S5	*10.4*	*12.8*	*1.23*	*293*	*115.3*	*408.3*	*1.39*

It is observed that calculated values of the energy absorption index were compatible with deflection ductility index for the corresponding tested specimens. It can be noticed that using tapered slab caused increase in the ductility by 11.42%, 21.78% for slab with positive haunch (S2 specimen) and 29.14%, 26.88% for slab with negative haunch (S3 specimen) when compared with the prismatic slab (S1 specimen) for deflection ductility index (μd) and energy absorption index (EAI), respectively. The higher ductility for S3 specimen with related to S1 specimen can be attributed to the lower stiffness of this slab. In addition, it is observed that S5 specimen have the lowest ductility due to the brittle failure for this slab as mentioned before.

4.3.2 Test Results of Two Span RC One Way Slabs (Group 2)

The following sections discuss the results of the experimental study for two span RC one-way slabs (group 2) including ultimate load, load-mid span deflection curves, the load of the first crack, the deflection and the crack width corresponding to the service load, crack pattern and mode of failure. Furthermore, deflection ductility and energy absorption index are also studied.

4.3.2.1 Load – Deflection Response and Ultimate Loads

A vertical dial gauge placed at the center of each span to register the mid-span deflection for slabs of this group. However, only the one that recorded maximum deflection has been depended in the analysis with the load capacity of that span. Figure 4-9 shows the load-midspan deflection relationship for all tested slabs of this group. Generally, there was insignificant deflection at the first stage of loading representing the uncrack stage.

As shown in Figure 4-9, a relatively small first similar branch for all specimens at early stages of loading is evident. With increasing the applied load, the slabs with tapered shape show increment in the deflection at the same load compared with the prismatic slab.

As expected, load-deflection response for slabs with fixed end support was stiffer than that for other support condition, however, in all support condition prismatic slabs was stiffer than non-prismatic slabs. This is attributed to the presence of the negative moment. Thus, the reduction in slab thickness whether that reduction was in mid span at positive moment (negative haunch) or in negative moment at the middle support (positive haunch), it effected the flexural rigidity and reduced the internal moment capacity.

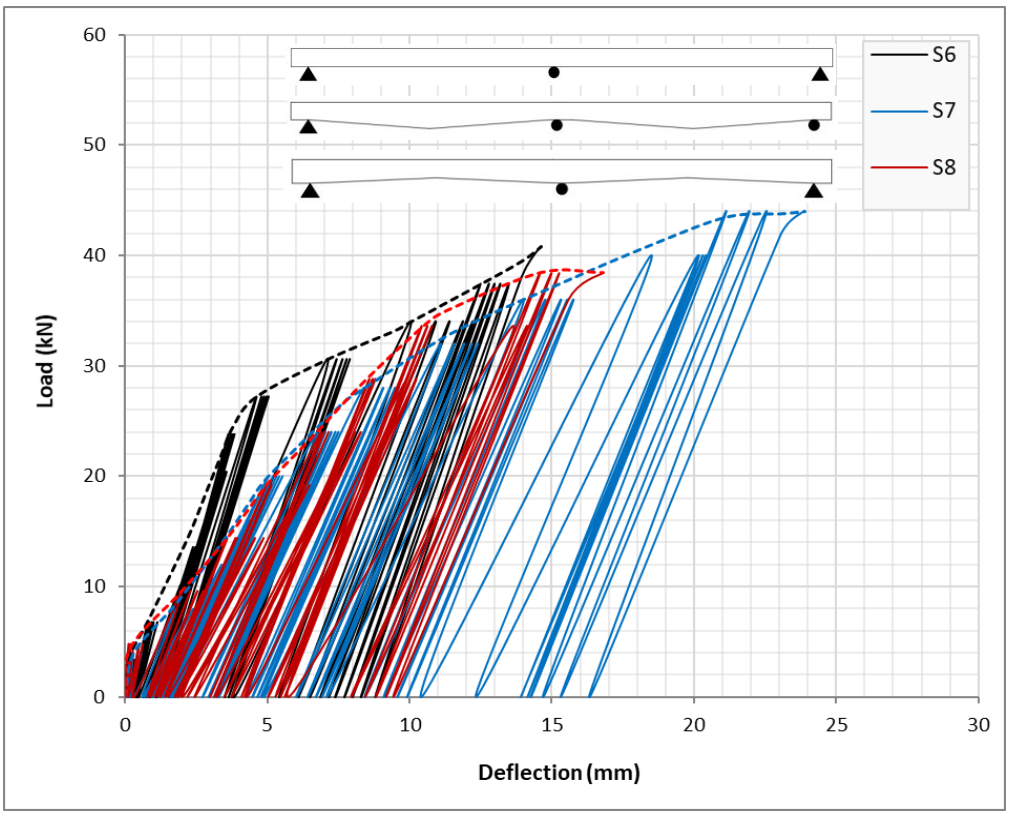

(a) simply supported slabs

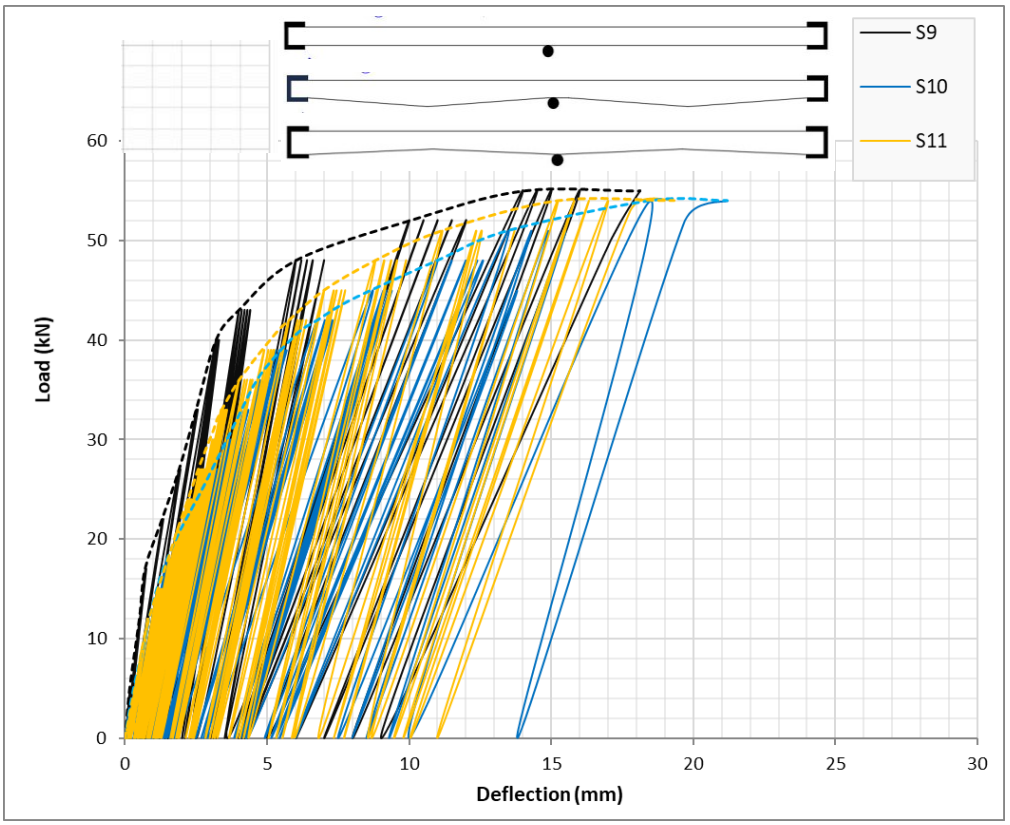

(b) fixed end supported slabs

Figure 4-9: Experimental Load - Midspan deflection curves for two span slabs.

It must be mentioned here that slabs of both groups have the same one span length, thus, the limitations of ACI 318-19 for immediate deflection due to maximum live load the same for all slabs. The ultimate load capacity (Pu), the mid span deflection at service load, and the mid span deflection at ultimate loads for two span slabs are presented in Table 4-5.

With regard to the support condition, it is found that using fixed at both end in S9 specimens increased the ultimate load capacity compared to simply support slab. On the other hand, providing tapered slab with positive or negative haunch have insignificant effect on the bearing capacity with respect to prismatic slab. While it caused significant increase in the deflection at service load compared to prismatic slab. In fact, the significant increase in the deflection at service load attributed to the reduction in slab thickness at critical section (maximum positive or negative moment) be providing tapered shape which effect the rigidity of slabs.

Table 4-5: Ultimate load capacity and deflection at mid span for for two span slabs.

Specimens designation	*Ultimate load Pu (kN)*	*Deflection at service load* δs (mm)*	*Increment in deflection at service load %*	*Deflection at ultimate load δu (mm)*
S6	*41*	*4 **	*control*	*14.62*
S7	*43*	*7.5 **	*87.5*	*23.9*
S8	*39*	*6.5 **	*62.5*	*16.8*
S9	*55*	*2.5*	*control*	*18*
S10	*54*	*4 **	*60*	*21.2*
S11	*54*	*3.3*	*32*	*19.32*

* Assumed service load = 60% from ultimate load of each slab

** Did not satisfy the limitations of ACI 318-19 [21] for immediate floors deflection which is 3.61 mm

4.3.2.2 Cracking Behavior and Modes of Failure

There was difference in the way that the cracks were formed for two span slabs in comparison with slabs of the first group. When the applied load reached the first cracking load, which was ranging between about 12.5% to 16.7% of the ultimate load, the first crack was observed in the critical tension face. After that, flexural

cracks developed and formed parallel to that crack and slowly propagated throughout the thickness of the slab.

A further increase in the load magnitude or the number of cycles of the repeated load led to more reduction in the stiffness of the slab models (plastic stage). Then all specimen of this group failed in a flexural mode of failure. That occurs after the rapidly increased in the width of some cracks at sagging and hogging regions, which mean that the tensile steel in the sagging and hogging regions were yielded. Following the yielding of tensile steel, crushing of concrete occurred at the top face of the specimen in the mid-span section and at the bottom face over the middle support. Photos of the control S9 specimen at failure are shown in Figure 4-10.

Failure of mid-span section (sagging region)

Failure of section over central support (hogging region)

Figure 4-10: Photos of the control S9 specimen at failure

Observations of cracks development were marked along the whole length of the slabs at the different load steps. Figures (4-11) and (4-12) shows the cracks pattern and failure modes obtained for simply supported slab and fixed end slabs of this group respectively.

a) Prismatic slab (S6 specimen)

b) Non-prismatic slab with positive haunch (S7 specimen)

c) Non-prismatic slab with negative haunch (S8 specimen)

Figure 4-11: Cracks pattern at failure for simply supported two span slabs

a) Prismatic slab (S9 specimen)

b) Non-prismatic slab with positive haunch (S10 specimen)

c) Non-prismatic slab with negative haunch (S11 specimen)

Figure 4-12: Cracks pattern at failure for fixed end support two span slabs

The experimental first cracking load (Pcr), width of first crack and mode of failure for each tested slabs of this group are presented in Table 4-6.

Table 4-6: Experimental first cracking load and width with failure mode for two span slabs.

Specimens designation	First cracking load Pcr (kN)		Crack width at servic load for the first crack (mm) *	Modes of failure
	Sagging region	Hogging region		
S6	5.75	5	0.30	Flexural
S7	6.2	4	0.30	Flexural
S8	5	7	0.45 **	flexural
S9	7	6	0.35	flexural
S10	7.75	5.5	0.38	flexural
S11	6.5	8	0.50 **	flexural

* Assumed service load = 60% from ultimate load of each slab

** Did not satisfy the limitations of ACI 318-19 [21] for maximum crack width which is 0.4 mm

From table 4-6 It is observed that the increase in slab depth caused increase in the required load for develop the first crack and vice versa. Thus, providing non-prismatic slab with negative haunch reduced the first cracking load at sagging region while it increased at hogging region. This is attributed to the change in the concrete depth at critical section which effect the moment of inertia and rigidity.

Similar to the behavior of one span one-way slabs, it is found that, the first crack width was almost 0.02 mm for slabs of this group. From Table 4-6 it is clear that providing cross section with negative haunch for both types of support condition caused an increase in the width of the first crack at service load more than the accepted limits of ACI 318-19.

4.3.2.3 Ductility

As discussed in the one span slab, two ductility definitions were explored here: Deflection ductility index (μd), and Energy absorption index (EAI). The results of deflection ductility index and energy absorption index with all the parameters that required to determined them for slabs of this group are presented in Table 4-7.

Table 4-7: Ductility index for two span slabs.

Beam designation	Yield deflection δy (mm)	Deflection at Ultimate load δu (mm)	Deflection ductility index μd	Elastic area A1 (kN.mm)	Plastic area A2 (kN.mm)	Total area A1+A2 (kN.mm)	Energy absorption index EAI
S6	9.5	14.62	1.53	217.5	189	406.5	1.86
S7	15.33	23.9	1.56	366	356	722	1.97
S8	11.33	16.8	1.48	230	204	434	1.88
S9	6.2	18	2.9	194	628	822	4.23
S10	8	21.2	2.65	237	670	907	3.8
S11	7	19.32	2.76	207	635	842	4.06

It is observed that calculated values of the energy absorption index were almost compatible with deflection ductility index for the corresponding tested specimens. It can be noticed that using tapered slab instant of prismatic slab have insignificant effect on the ductility index.

It must be mentioned that the higher ductility for fixed end specimens with related to simply support specimens could be attributed to the higher stiffness of this slab at the first stage of loading and vice versa at plastic stage of loading.

5

Chapter 5
FINITE ELEMENT ANALYSIS

5.1 Introduction

In this chapter, a comparison study is presented among the differences between the results of the three-dimensional nonlinear finite element (FE) study and the results of the laboratory work to verify the validity of the proposed FE model by study the appropriateness of elements types, material properties, the convergence study, and the real constants of the representing one-way slab models.

ABAQUS/Standard 2017 that is an advanced three-dimensional finite element computer program, was utilized to perform a nonlinear finite element analysis to analyze the behavior of all slabs that were conducted experimentally in the current study.

The details of the developed FE model will be presented first, which includes the element types, the constitutive model, the mesh size, and the boundary conditions of each component.

5.2 Element Type and Material Properties

In order to model the real behaviour of RC slabs, it is recommended that concrete be modelled with eight-nodded linear 3D brick solid element with reduced integration (C3D8R) [33] as shown in Figure 5-1a. This element type provides reliable solution to most applications. Each 3D solid element has eight nodes with three degree of freedom per node. It can be used for both linear and complex non-linear analysis involving contact, plasticity, and large deformations. On the other hand, 2-nodded linear truss elements (T3D2) as shown in Figure 5-1b was used to model steel bar reinforcements. Similar to concrete slab, the three-dimensional solid element (C3D8R) was chosen to model the steel plates in both loading and supporting positions.

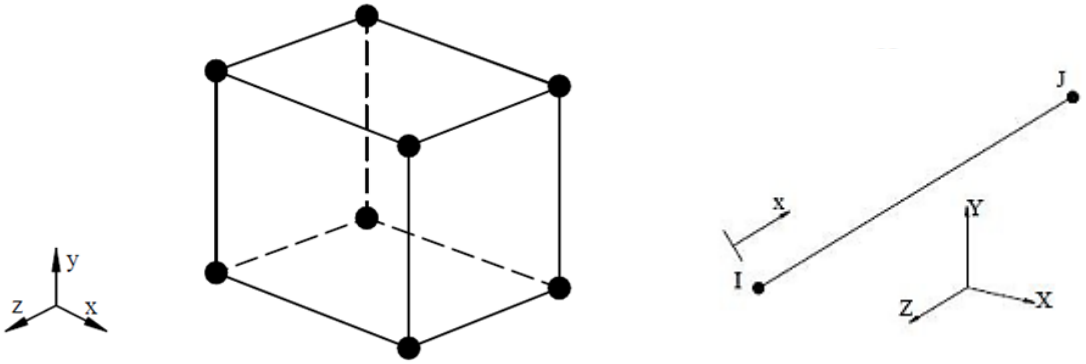

(a) C3D8R element [33] (b) T3D2 truss element [34]

Figure 5-1: Element type used in FE simulation.

Among the constitutive models for simulating the behaviour of concrete, the concrete damaged plasticity model (CDP) that ABAQUS offers was chosen. Details of the CDP model, including the behaviour and properties of the concrete and the other material used in this study are shown in **Appendix B.**

5.3 Model Geometry and Boundary Conditions

3D simulations were performed to get an accurate approximation of the overall behaviour and failure mode for RC slabs. By considering symmetry of the

specimens, only one quarter of the specimens was used for the simulations. Figure 5-2 gives a 3D view of the geometry of the FE model developed for the prismatic slabs of both groups. The X-axis is along the longitudinal direction of the slab, and the Y-Z plane represents the cross section of the slab.

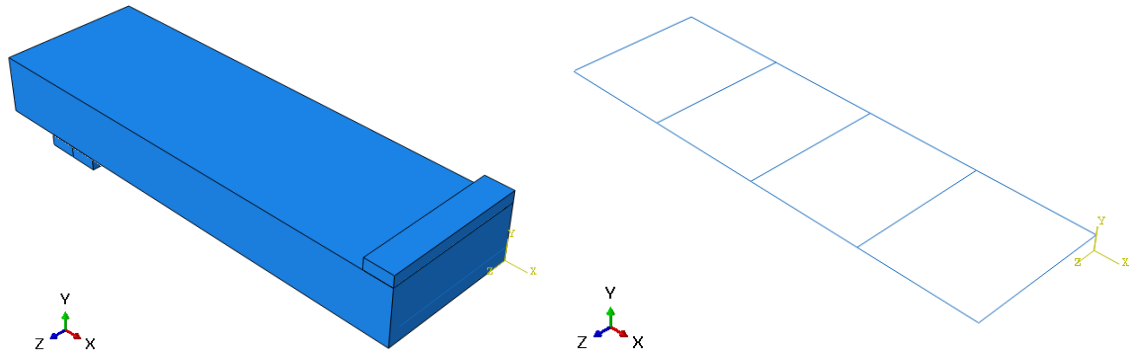

(a) S1 specimen (one span slab)

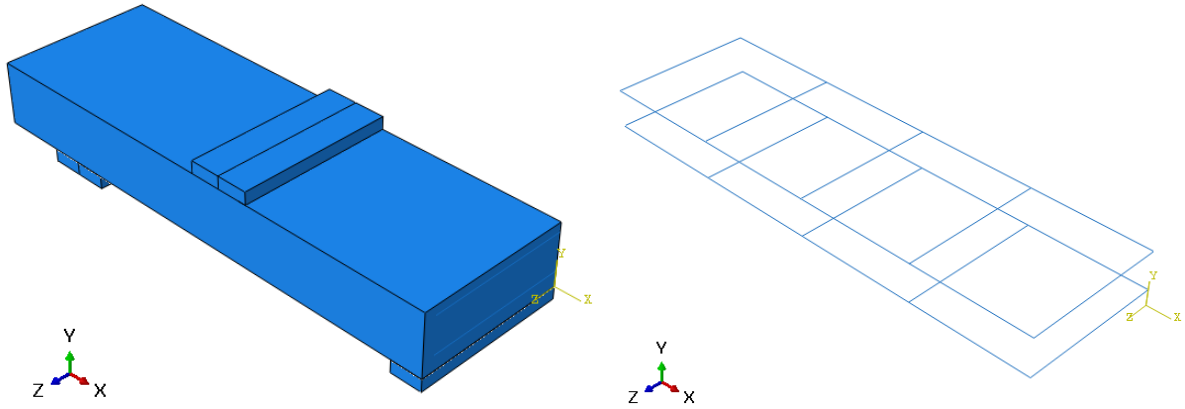

(b) S6 specimen (two span slab)

Figure 5-2: 3D view of the FE model of RC slab.

The embedded method was adopted to simulate the bond between the concrete and the reinforcement. In this constraint, steel reinforcement bars were selected as embedded region, while concrete served as the host region. This constraint simulates a perfect concrete–steel bond. Steel plates in both loading and supporting positions are connected to the slab specimen using the ‘‘tie’’ option, which means that parts cannot be disconnected during loading.

For simply supported slabs, a simple support restraining translations in the y-direction is imposed at one end of slabs. While for slabs with fixed ends, restraining in all direction is imposed. The actual constraints are inserted along the width of the slab on a line placed on the middle of the steel plates.

Since FE commercial software can be high demanding in computational time two symmetry planes are taken into consideration. The first one is placed in the centre of the slab along its width. For this symmetry plane a constraint along the x-axis is consider. Moreover, a second plane is considered along the length and here the translation along the z-axis is constrained.

The RC slab were analysed using quasi-static analysis in ABAQUS/Standard. In such analysis, the repeated loads were applied on the finite element models similarly as in the experimental test as a uniformly applied pressure on the bearing plate(s). Besides, the protocol of the repeated loads was defined in advance using tabular type amplitudes.

Figure 5-3 gives details regarding the typical boundary conditions of the specimens used for the simulations.

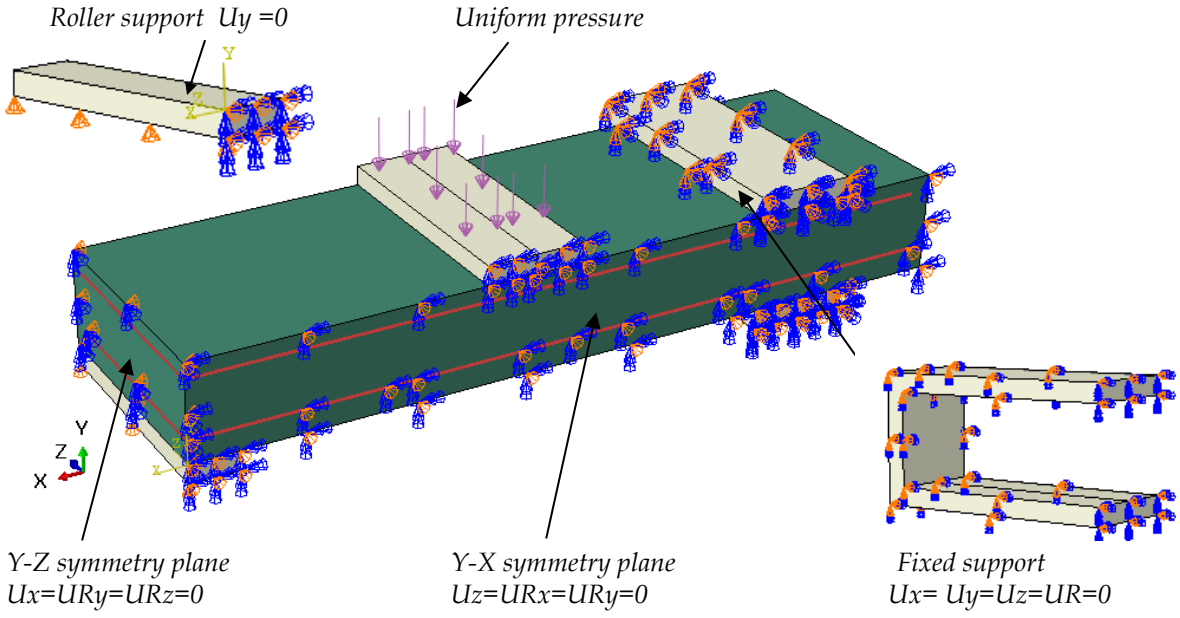

Figure 5-3: Applied load and boundary conditions of modelled slabs (S9 specimen).

5.4 Meshing and Convergence Analysis

The main aim of the convergence study is to select the proper mesh size of the model with a minimum number of elements and maximum convergence with the results of the experimental test. This is practically achieved when the decreasing in the mesh size has a negligible effect on the results by using control specimen of the first group with the same material properties were modelled with a decrease in the element sides 50, 35, 25, 15, 10 and 7.5 mm in all-axis.

The mid-span deflection for the mentioned specimen with different mesh size was observed at the same applied load level of 20 kN. As shown in Figure 5-4 convergence study, showed that the difference can be ignored when the number of elements increased from 20000 elements (mesh size of 10 mm) to 45000 elements (mesh size of 7.5 mm), therefore; the 10 mm model is adopted for all tested specimens in all-direction as shown in Figure 5-5. Also, a mesh size of 10 mm was adopted for both steel reinforcement bars and plates.

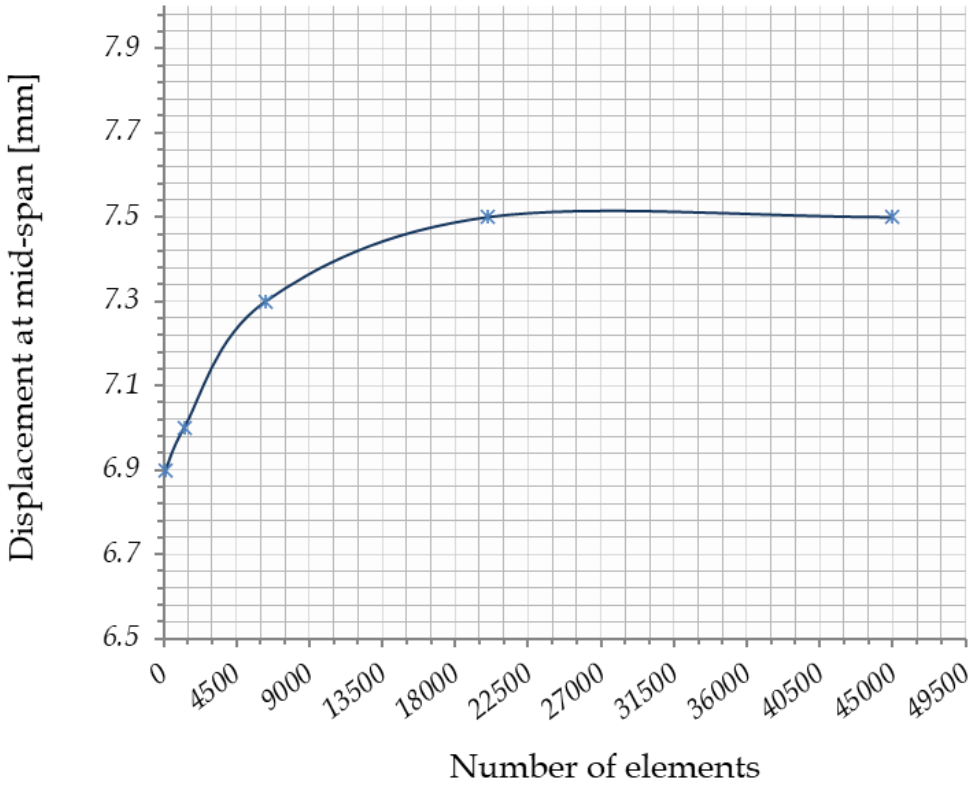

Figure 5-4: Convergence analysis. Imposed load equal to 20 kN.

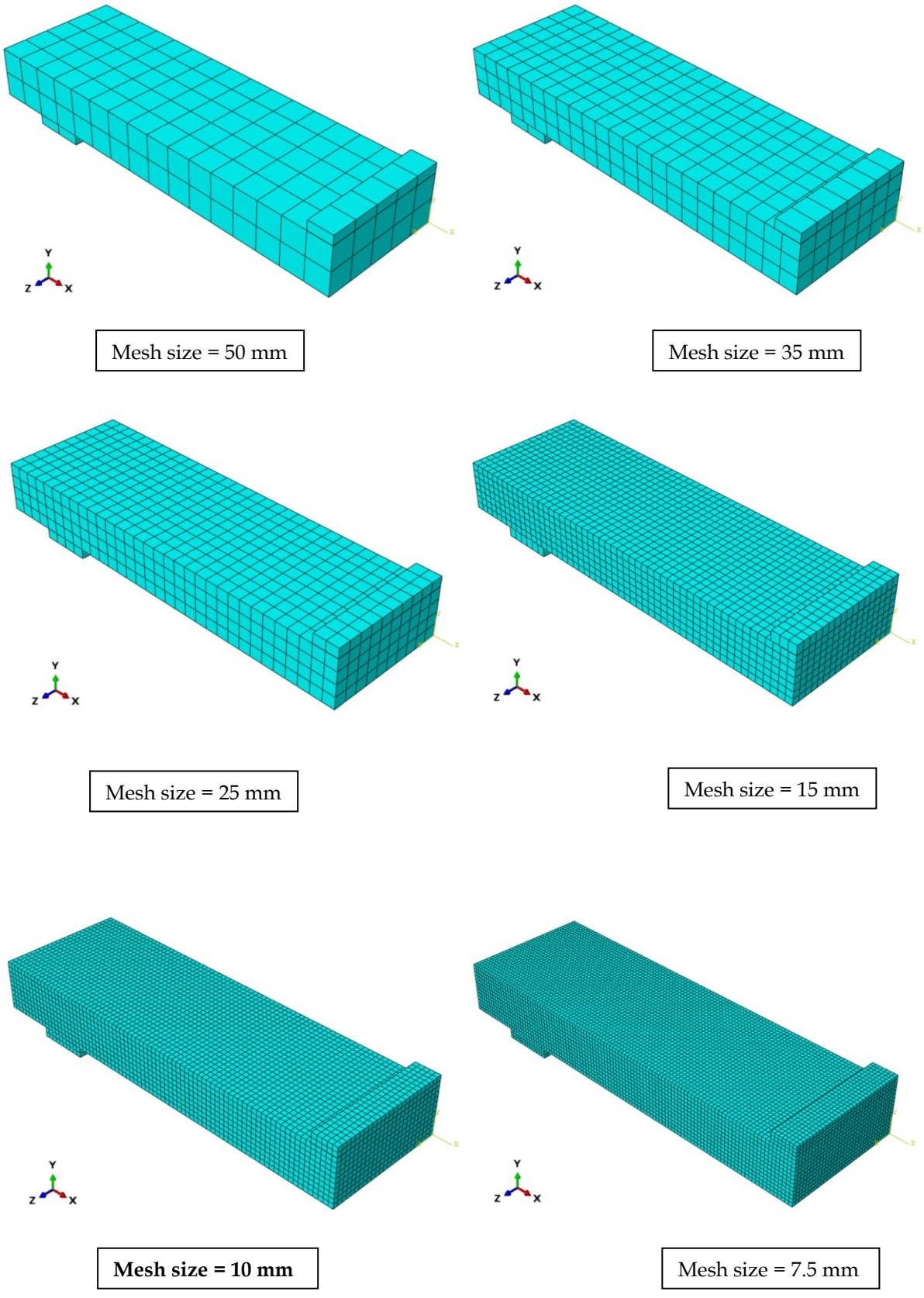

Figure 5-5: Typical mesh applied for the RC slabs of first group (S1 specimen).

5.5 Finite Element Analysis Results and Discussion

The load-deflection relationship reflects the behavior of the studied members during the entire loading history. Therefore, it is an important indication of the validity of the FE model. The load–midspan deflection responses obtained from FEM were compared with the experimental results for slabs of the first and second groups, as shown in Figures 5-6 and 5-7 respectively. The load–midspan deflection predicted by the FEM was generally similar to the experimental data. However, it exhibited stiffer responses than the corresponding ones obtained from the experimental specimens. There could be many reasons behind higher stiffness in FEM. The most important reason is the development of micro cracks due to dry shrinkage, concrete handling, environmental effects, and so on, in case of the experiments. FEM does not include such micro cracks in the simulations [35]. Another possible reason for the stiffer initial load–midspan deflection response of the numerical slabs is the way rebars bonds were modelled. As stated earlier in geometry model, the embedded region constraint that was used in ABAQUS to model the concrete– rebars interaction simulates a perfect bond. Since the actual bond is not perfect in reality, this idealization may also contribute to the spurious initial higher stiffness in the numerical model.

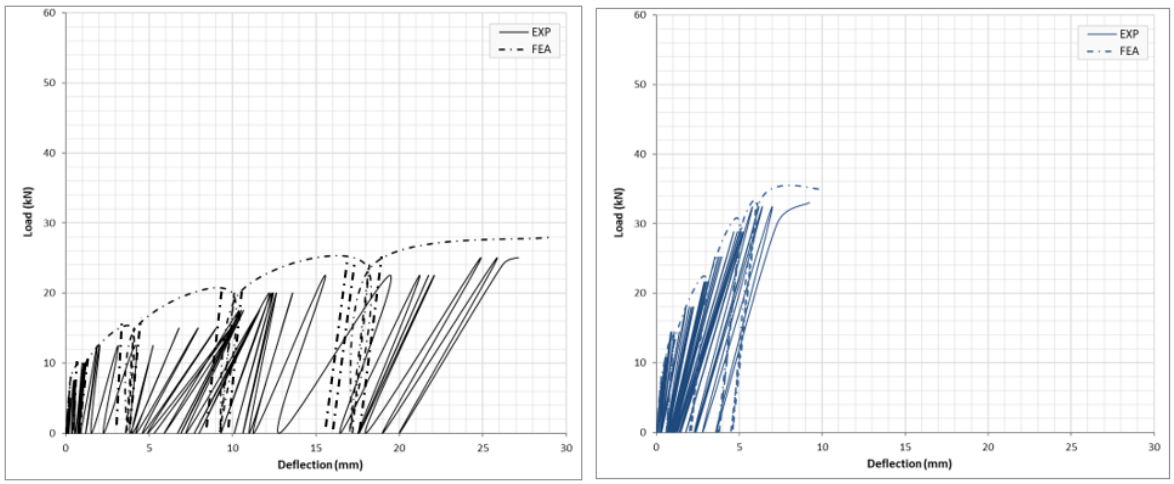

(a) S1 specimen *(b) S2 specimen*

Figure 5-6: Experimental and numerical load-midspan deflection curves for one-span slabs.

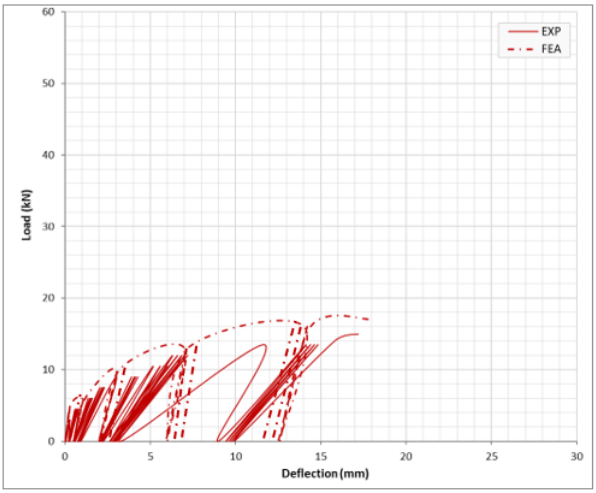

(c) S3 specimen

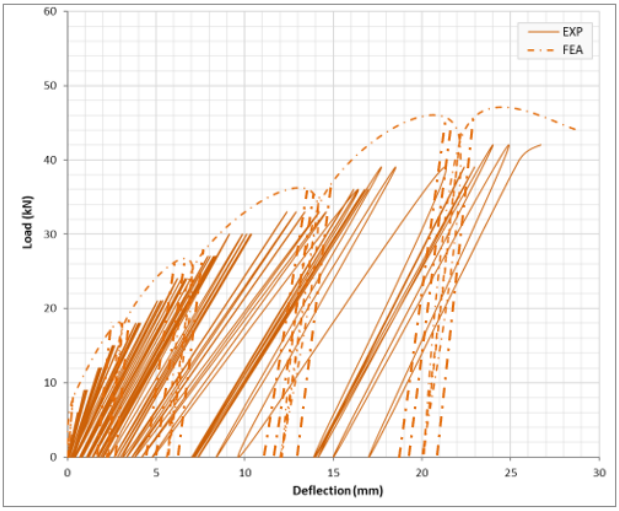

(d) S4 specimen

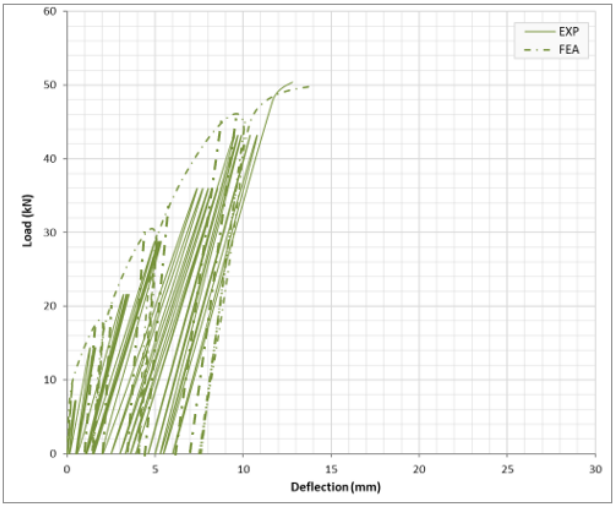

(e) S5 specimen

Figure 5-6: Continued.

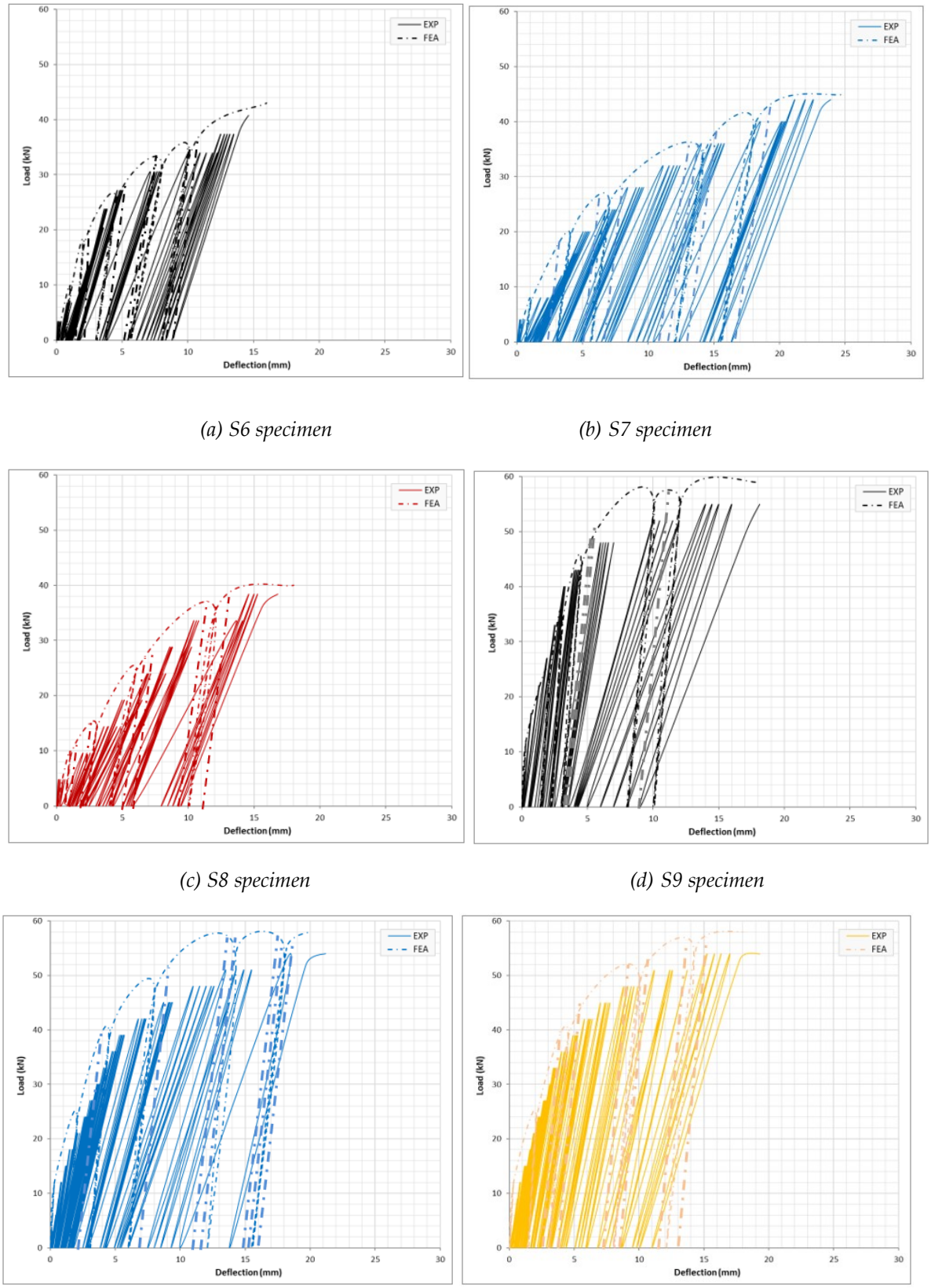

(a) S6 specimen (b) S7 specimen

(c) S8 specimen (d) S9 specimen

(e) S10 specimen (f) S11 specimen

Figure 5-7: Experimental and numerical load-midspan deflection curves for two-span slabs.

Table 5-1 presented the summary of FEM and experimental results. FEM was able to capture the minor changes in load–midspan deflection response caused by the repeated loads. The average difference in results was about 5.9% increase in ultimate loads, a 5.37 % decrease in the maximum deflection at service loads, and a 4.1% increase in the maximum deflection at ultimate loads. However, it can be inferred that the results predicted by FEM were in good agreement with the experimental results. The typical displacement profile for slab by FEA is shown in Figure 5-8.

Table 5-1 : Summary of FEM and experimental results.

Slab designation	*Ultimate load Pu (kN)*		*Deflection at service load* δs (mm)*		*Deflection at ultimate load δu (mm)*		*(FEM / Exp) ratio*		
	Exp	*FEM*	*Exp*	*FEM*	*Exp*	*FEM*	*Pu*	*δs*	*δu*
S1	*25*	*28*	*6*	*5.3*	*27.15*	*29*	*1.12*	*0.883*	*1.068*
S2	*33*	*35*	*2.3*	*2.2*	*9.24*	*10*	*1.06*	*0.956*	*1.082*
S3	*15*	*17*	*3*	*3*	*17.19*	*18*	*1.13*	*1*	*1.047*
S4	*42*	*44*	*6.75*	*7*	*26.7*	*29.2*	*1.047*	*1.037*	*1.093*
S5	*50.4*	*51*	*5.3*	*5.2*	*12.8*	*14*	*1.01*	*0.981*	*1.093*
S6	*41*	*43*	*4*	*4.2*	*14.62*	*16*	*1.048*	*1.05*	*1.094*
S7	*43*	*45*	*7.5*	*7*	*23.9*	*25*	*1.046*	*0.93*	*1.046*
S8	*39*	*40*	*6.5*	*5.5*	*16.8*	*18*	*1.025*	*0.846*	*1.071*
S9	*55*	*59*	*2.5*	*2.5*	*18*	*18.2*	*1.072*	*1*	*1.01*
S10	*54*	*58*	*4*	*3.5*	*21.2*	*20*	*1.074*	*0.875*	*0.943*
S11	*54*	*58*	*3.3*	*3*	*19.32*	*18.1*	*1.074*	*0.909*	*0.936*

* Assumed service load = 60% from ultimate load of each slab

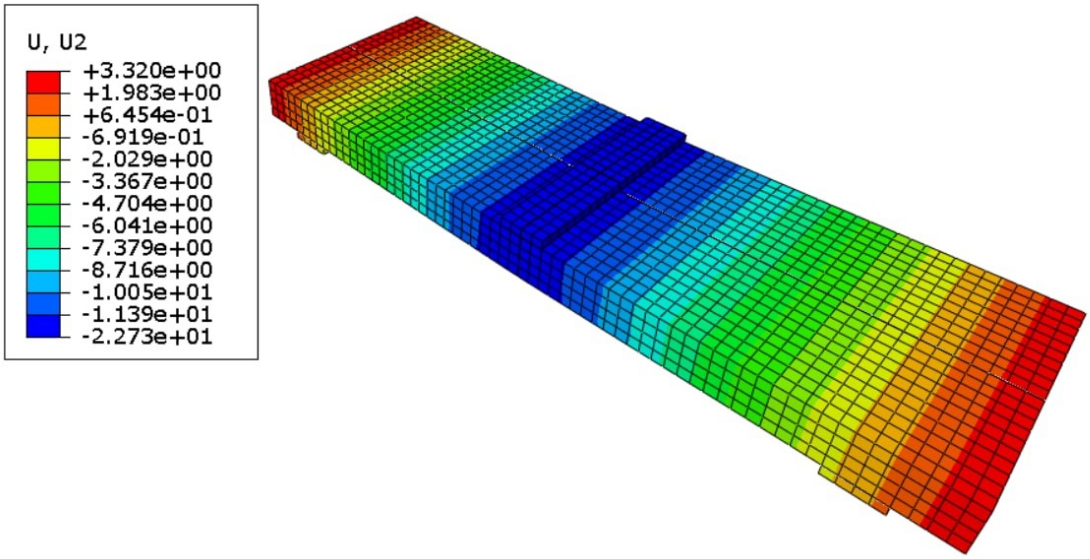

Figure 5-8: displacement profile in vertical direction, mm (S1 specimen)

5.6 Parametric Study

After the FEA of one-way reinforced concrete slabs showed sufficient correlation with the outcomes of experimental program. A comparison with applying static (monotonic) load that was not considered in the experimental program was studied numerically using the same adopted model. Only one specimen from each group was selected for that comparison. The load–midspan deflection responses obtained from FEM for S1 and S6 specimens under repeated load were compared with the numerically results for these slabs under static load, as shown in Figure 5-9.

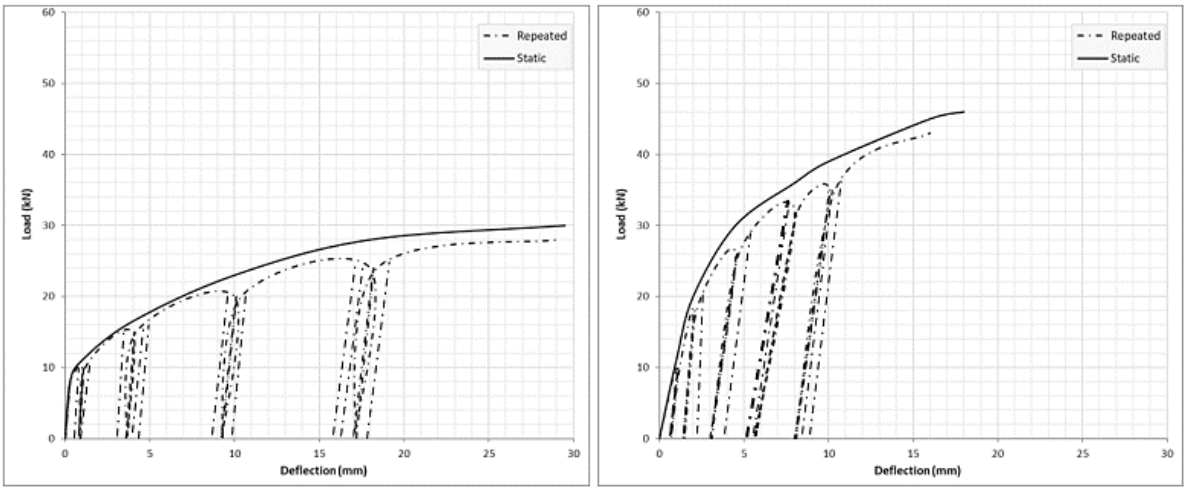

(a) S1 specimen *(b) S6 specimen*

Figure 5-9: Numerical load-midspan deflection curves for slabs under static and repeated load.

The load–midspan deflection predicted for models under static load was generally similar to that under repeated load. However, it exhibited stiffer response at plastic stage of loading. Test results revealed that applying static load instead of five cycles of repeated load to the RC one-way slab specimens led to increasing in the ultimate load capacity as it is clear in Table 5-2. This ensures the efficiency of adopted repeated load strategy to consider the fatigue phenomenon related to such type of load.

Table 5-2: Numerical load, midspan deflection for slabs under static and repeated load.

Slab designation	Ultimate load kN		deflection at ultimate load mm	
	static	repeated	static	repeated
S1	30	28	29.5	29
S6	46	43	18	16

6

Chapter 6
CONCLUSIONS AND RECOMMENDATIONS FOR FUTURE WORKS

6.1 Introduction

In the previous chapters, an experimental work together with a finite element analysis for RC slabs had been performed. Both experimental and numerical results using ABAQUS software showed that providing RC slabs with non-prismatic cross section have varying effect on the overall behaviour and ultimate strength depends on many parameters.

In this chapter, conclusions from the experimental and numerical results will be presented, also, some suggestions for future addition works will be offered.

6.2 Conclusions

Based on the results obtained from the experimental work and finite element analysis by ABAQUS program for RC slabs with prismatic and non-prismatic cross section, the following conclusions can be stated within the scope of this study:

1- Load-deflection response for non-prismatic simply supported one span slab with positive haunch is stiffer than the prismatic one. This behavior is due to the increase in the cross-sectional area at the critical section (mid span) and that enhanced the flexural rigidity and moment capacity, and vice versa for negative haunch slab.

2- The load capacity of slab increases by 32% when using positive haunch in simply supported one span slab. While for negative haunch, the reduction in the load capacity is 40% from the ultimate load of the prismatic slab. That is attributed to the reduction in the concrete depth at the critical section which effect the moment capacity.

3- Providing positive haunch caused decrease in the deflection at both service and ultimate load compared to prismatic simply supported one span slab

4- Reduction in the first cracking load for non-prismatic simply supported one span slab with negative haunch is 51.08% with respect to the reference slab. While, non-prismatic slab with positive haunch shows a significant increase in the first cracking load.

5- Using tapered one span slab caused increase in the ductility by 11.42%, 21.78% for slab with positive haunch and 29.14%, 26.88% for slab with negative haunch when compared with the prismatic slab for deflection ductility index (μd) and energy absorption index (EAI), respectively.

6- With regard to the support condition, it is found that using fixed at both ends have a significant effect on increasing the ultimate load capacity compared to simply support one span slab.

7- Providing tapered slab with positive or negative haunch have insignificant effect on the bearing capacity with respect to prismatic continuous slab.

8- Providing tapered continuous slab caused significant increase in the deflection at service load compared to prismatic slab. In fact, the significant increase in the deflection at service load attributed to the reduction in slab thickness at critical section (maximum positive or negative moment) by providing tapered shape which effect the rigidity of slabs.

9- Providing negative haunch cross section for continuous slab for both types of support condition caused an increase in the width of the first crack at service load more than the accepted limits of ACI 318-19.

10- Using tapered continuous slab instant of prismatic slab have insignificant effect on the ductility index

11- Values of the energy absorption index were almost compatible with deflection ductility index for the corresponding tested specimens.

12- It is recommended to use prismatic continuous one-way slabs rather than non-prismatic ones because of higher stiffness and almost the same load carrying capacity

13- The 3D finite element analysis, based on the CDP model by ABAQUS package is valid for the analysis of RC slabs. The general response of load-deflection curves, the ultimate load, and the mid span deflection of the studied reinforced slabs predicted by FEM were in good agreement with the experimental results. The average difference in results was about 5.9% increase in ultimate loads, a 5.37 % decrease in the maximum deflection at service loads, and a 4.1% increase in the maximum deflection at ultimate loads

14- Applying static (monotonic) load instead of five cycles of repeated load to the RC one-way slab specimens led to increasing the ultimate load capacity with difference of 7%

6.3 Recommendations for Future Works

Based on the findings of this study, the following suggestions for future investigations are drawn:

1- Investigate the flexural behaviour of reinforced concrete one-way slabs with non-prismatic cross section with different levels of reinforcement ratio.

2- Strengthening and rehabilitation of reinforced concrete slabs with non-prismatic cross section by different types of FRP products.

3- Investigate the structural behaviour of reinforced concrete thick slabs with non-prismatic cross section.

4- Investigate the structural behaviour of reinforced concrete two-way slabs with non-prismatic cross section.

R

REFERENCES

1- Balduzzi, Giuseppe, Mehdi Aminbaghai, Elio Sacco, Josef Füssl, Josef Eberhardsteiner, and Ferdinando Auricchio. "Non-prismatic beams: a simple and effective Timoshenko-like model." International Journal of Solids and Structures 90 (2016): 236-250.

2- Russell, Henry G., Arthur R. Anderson, Jack O. Banning, Irwin G. Cantor, Ramon L. Carrasquillo, James E. Cook, Gregory C. Frantz et al. "State-of-the-art report on high-strength concrete." ACI Committee 363 (1997): 92.

3- Tayfur, Yadgar, Antony Darby, Tim Ibell, John Orr, and Mark Evernden. "Serviceability of non-prismatic concrete beams: Combined-interaction method." Engineering Structures 191 (2019): 766-774.

4- Tayfur, Yadgar Rafiq. "Optimisation for serviceability of fabric-formed concrete structures." PhD diss., University of Bath, 2016.

5- Orr, John, Anthony P. Darby, Timothy Ibell, M. C. Evernden, and Mike Otlet. "Concrete structures using fabric formwork." Structural Engineer 89 (2011): 20–26.

6- Song, Zhengyang, Thomas Frühwirt, and Heinz Konietzky. "Characteristics of dissipated energy of concrete subjected to cyclic loading." Construction and Building Materials 168 (2018): 47-60.

7- Tanaka, K., T. Nawa, H. Hashida, and J. H. Jeon. "Effect of repeated load on micro structure and carbonation of concrete and mortar." In Eighth

International Conference on Durability of Building Materials and Components, 8 dbmc, pp. 256-265. 1999.

8- Toshniwal, Shubham. "Shear Analysis of Non-Prismatic Concrete Beams." Master thesis, Delft University of Technology, 2019.

9- Tena-Colunga, Arturo, Hans I. Archundia-Aranda, and Óscar M. González-Cuevas. "Behavior of reinforced concrete haunched beams subjected to static shear loading." Engineering Structures 30.2 (2008): 478-492.

10- Aziz, Ali Hameed, Hassan Falah Hassan, and Faisal Muayad Abdul Razzaq. "Experimental study on shear behavior of reinforced self-compacted concrete tapered beams." Civ. Environ. Res 8.8 (2016): 11-22.

11- Tan, Kiang Hwee. "Design of non-prismatic RC beams using strut-and-tie models." Journal of Advanced Concrete Technology 2.2 (2004): 249-256.

12- Archundia-Aranda, Hans I., and Arturo Tena-Colunga. "Cyclic behavior of reinforced concrete haunched beams failing in shear." Memorias, 14th World Conference on Earthquake Engineering, Beijing, China, Artículo. No. 12-01. 2008.

13- Nghiep, Vu Hong. Shear design of straight and haunched concrete beams without stirrups. Technische Universität Hamburg, PhD thesis, 2011.

14- Nimnim, Haider Talib, Ali Talib Jassim, and Ali Amer Abdul Mohsen. "Structural behavior of reinforced reactive powder concrete tapered beams." Practice Periodical on Structural Design and Construction 24.2 (2019): 04019002.

15- Archundia-Aranda, Hans I., Arturo Tena-Colunga, and Alejandro Grande-Vega. "Behavior of reinforced concrete haunched beams subjected to cyclic shear loading." Engineering Structures 49 (2013): 27-42.

16- Dawood, Mustafa B., and M. H. Abdulkhaleq. "Structural behavior of non-prismatic reactive powder concrete (RPC) continuous members under effect of static and repeated loads." Int. J. Sci. Eng. Res 8.1 (2017): 800-806.

17- Toshniwal, Shubham. "Shear Analysis of Non-Prismatic Concrete Beams.", Master thesis, Delft University of Technology, Netherlands (2019).

18- Sivagamasundari, R., and G. Kumaran. "A comparative study on the flexural behaviour of one-way concrete slabs reinforced with GFRP reinforcements and conventional reinforcements when subjected to monotonic and repeated loading." The Open Civil Engineering Journal 2.1 (2008).

19- Al-Sulayvani, Bayar J., and Diyar N. Al-Talabani. "Strengthening and repair of circular RC slabs with openings using CFRP strips under repeated loading." Construction and Building Materials 84 (2015): 73-83.

20- Al-shaarbaf, Ihsan AS, Amar Abbas Ali, and Mohammed A. Ahmed. "Experimental Behavior of Self Compacted Concrete Voided Slab Strips Under Repeated Loads." 2019 12th International Conference on Developments in eSystems Engineering (DeSE). IEEE, 2019.

21- ACI Committee 318, Building Code Requirements for Structural Concrete and Commentary. ACI, 2019.

22- IQS No. 5, 1984,"Portland Cement", Iraqi Specification Standards, Central Agency for Standardization and Quality Control, Planning Council, Baghdad, IRAQ.1984.

23- IQS No. 45, 1984, " Aggregate from natural sources for concrete and construction", Iraqi Specification Standards, Central Agency for Standardization and Quality Control, Planning Council, Baghdad, IRAQ.1984.

24- ASTM C494 / C494M - 17, "Standard Specification for Chemical Admixtures for Concrete," American Society for Testing and Materials, 2017.

25- ASTM A1064 / A1064M - 18a, "Standard Specification for Carbon- Steel Wire and Welded Wire Reinforcement, Plain and Deformed, for Concrete," American Society for Testing and Materials, 2018.

26- ASTM C192, "Standard practice for making and curing concrete test specimens in the laboratory," Annual Book of American Society for Testing Materials Standards, vol. 4, 2007.

27- BS 1881: Part 116; ''Method for Determination of Compressive Strength of Concrete Cubes,'' British Standards Institution, 1989.

28- ASTM C39/C39M-20. "Standard test method for compressive strength of cylindrical concrete specimens." (2020).

29- ASTM C78-10, "Standard test method for flexural strength of concrete (using simple beam with third-point loading)," in American society for testing and materials, 2010, pp. 19428-2959.

30- ASTM C496-11,“Standard Test Method for Splitting Tensile Strength of Cylindrical Concrete Specimens.” ASTM International, West Conshohocken, PA, 2011, DOI: 10.1520/C0496_C0496M-11."

31- T. J. Sullivan, and G. M. Calvi and and M. J. N. Priestley, "Initial stiffnes versus secant stiffness in displacement-based design," in 13th World Conference of Earthquake Engineering (WCEE), 2004.

32- M. J. N. Priestley and and R. Park, "Strength and ductility of concrete bridge columns under seismic loading," Structural Journal, vol. 84, no. 1, p. 61–76, 1987.

33- Bahij, Sifatullah, et al. “Numerical investigation of the shear behavior of reinforced ultra-high-performance concrete beams,’’ Structural Concrete, PP. 305-317, 2018.

34- Wu, Yuanli. “Shear Strengthening of Single Web Prestressed Hollow Core Slabs Using Externally Bonded FRP Sheets,’’ M.Sc. Thesis, Windsor’s University, Canada, 2015.

35- Meng, Xianzhe. “Shear strengthening of prestressed hollow core slabs using externally bonded Carbon Fiber Reinforced Polymer sheets.", M.Sc. Thesis, Windsor’s University, Canada, 2016.

A

Appendix A
DESIGN OF REINFORCED CONCRETE SLABS

All slabs were design according to ACI-Code 318M-14. The control slabs for both groups were designed in such a way to ensure flexural failure with a tensile mode of failure.

One span slab (group 1)

The reference slab of this group reinforced by 3 Ø 8 mm longitudinal steel reinforcement at bottom with slab effective depth (d = 75 mm). Also, Ø 8 mm transverse steel reinforcement was provided each 200 mm at bottom of the short direction. The clear concrete cover was 20 mm. The yield strength for rebars (fy) equals 550 MPa. The target concrete compressive strength (fc') equals 35 MPa.

- Checking flexural capacity of the section

$$\rho = \frac{As}{b \times d} = \frac{3 \times 50.2}{500 \times 75} = 0.004$$

$$\beta_1 = 0.85 - 0.05\left(\frac{fc' - 28}{7}\right) \leq 0.65$$

$$\beta_1 = 0.8$$

$$\rho_t = 0.85\beta_1 \frac{f_{c\prime}}{f_y} \frac{\varepsilon_u}{\varepsilon_u + 0.005}$$

$$\rho_t = 0.0162 \qquad \therefore \rho < \rho_t$$ Tension controlled slab

$$a = \frac{As \times fy}{0.85fc' \times b} = \frac{3 \times 50.2 \times 550}{0.85 \times 35 \times 500} = 5.568\ mm$$

$$m_n = A_s \times f_y(d - \frac{a}{2})$$

$$m_n = 6.218\ kN.m$$

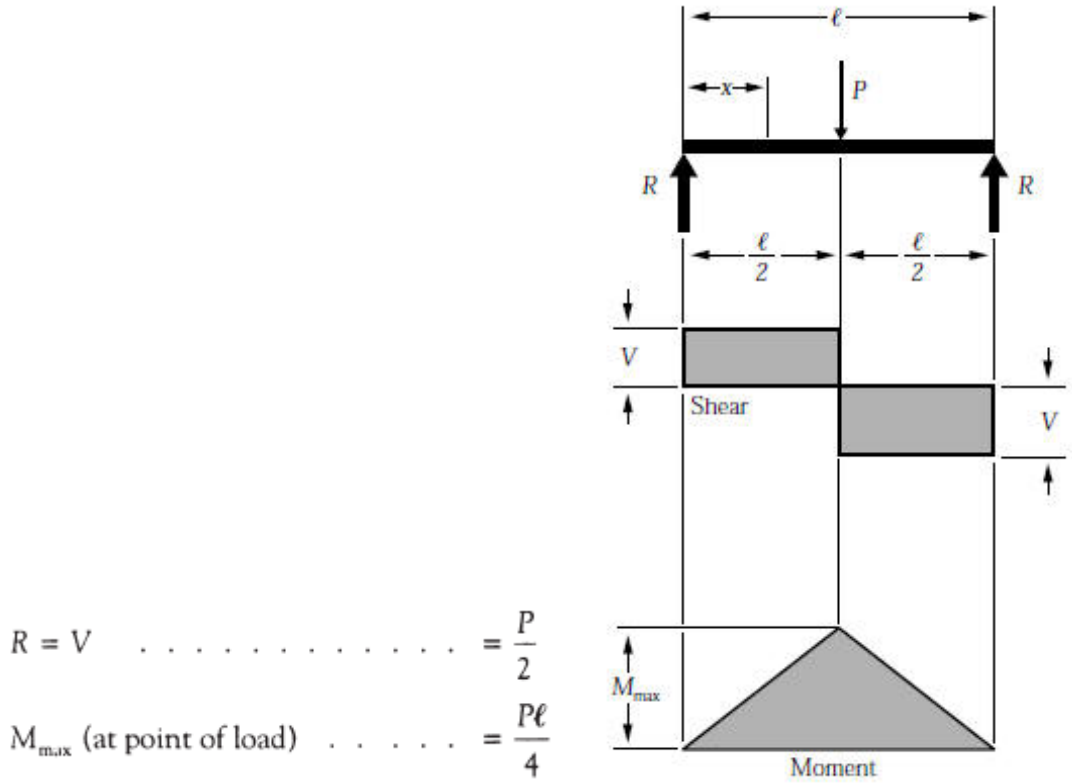

$R = V \quad . . . . . = \frac{P}{2}$

M_{max} (at point of load) $. . . . . = \frac{P\ell}{4}$

Figure A-1: Shear and bending moment diagrams for one span simply supported slabs

$m_{ext} = m_n$

From Figure A-1, it is clear that $m_{ext} = 0.325P$ (L = 1.3 m)

$0.325P = 6.218 \rightarrow P = 19.13\ kN$

- Checking shear capacity of the section

$V_c = 0.17\sqrt{f_{c'}}\ b_w \times d$

$V_c = 37.7\ kN$

$V_{ext} = V_n \qquad V_{ext} = 0.5\ P$

$0.5\ P = 37.7 \quad \rightarrow P = 75.4\ Kn$

$\therefore$ Shear failure load > Flexural failure load

$\therefore$ Flexural tension failure controls.

A.2 Two spans slab (group 2)

The reference simply supported slab of this group were 3000 mm long, 500 mm wide, and comprised two equal spans of 1300 mm each. Slab was tested to failure under two-point line loads, one in the mid of each span. Slab was reinforced by 3 Ø 8 mm longitudinal steel reinforcement at top and bottom, also Ø 8 mm transverse steel reinforcement was provided each 200 mm at top and bottom of the short direction of slab. The clear concrete cover was 20 mm. The yield strength for rebars (fy) equals 550 MPa. The target concrete compressive strength (fc′) equals 35 MPa.

- Checking flexural capacity of the section

$$\rho = \frac{As}{b \times d} = \frac{3 \times 50.2}{500 \times 75} = 0.004$$

$$\beta_1 = 0.85 - 0.05\left(\frac{fc' - 28}{7}\right) \leq 0.65$$

$$\beta_1 = 0.8$$

$$\rho_t = 0.85\beta_1 \frac{f_{c\prime}}{f_y} \frac{\varepsilon_u}{\varepsilon_u + 0.005}$$

$\rho_t = 0.0162 \qquad \therefore\ \rho < \rho_t$ Tension controlled slab

$$a = \frac{As \times fy}{0.85 fc' \times b} = \frac{3 \times 50.2 \times 550}{0.85 \times 35 \times 500} = 5.568\ mm$$

$$m_n = A_s \times f_y\left(d - \frac{a}{2}\right)$$

$$m_n = 6.218\ kN.m$$

$$R_1 = V_1 = R_3 = V_3 \quad = \frac{5P}{16}$$

$$R_2 = 2V_2 \quad = \frac{11P}{8}$$

$$V_2 = P - R_1 \quad = \frac{11P}{16}$$

$$V_{max} \quad = V_2$$

$$M_1 \quad = -\frac{3P\ell}{16}$$

$$M_2 \quad = \frac{5P\ell}{32}$$

$$M_x \text{ (when } x < a) \quad = R_1 x$$

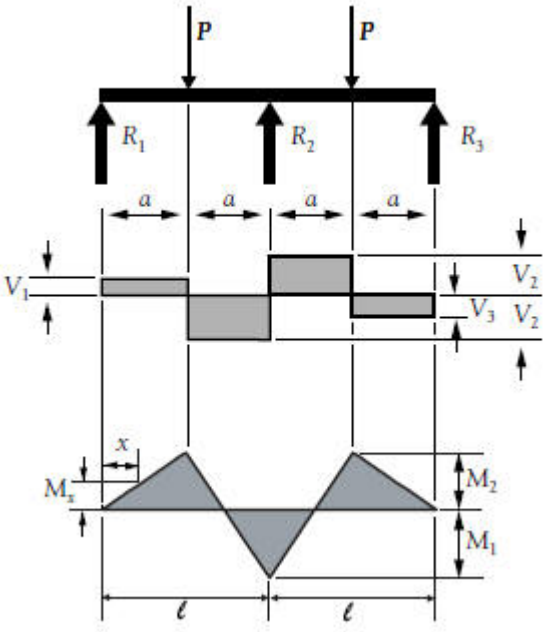

Figure A-2: Shear and bending moment diagrams for two spans simply supported slabs

From Figure A-2, it is clear that $m_{ext}(\text{max}) = 0.24375P$ (L = 1.3 m)

$0.24375P = 6.218 \rightarrow P = 25.51\ kN$

Checking shear capacity of the section

$V_c = 0.17\sqrt{f_{c'}}\, b_w \times d$

$V_c = 37.7\ Kn$

$V_{ext} = V_n \qquad V_{ext} = 0.6875\ P$

$0.6875\ P = 37.7 \rightarrow P = 54.8\ kN$

∴ Shear failure load > Flexural failure load

∴ Flexural tension failure controls.

Maximum allowable load that can be sustained by flexural and shear capacity of each slab are presented in Table A-1.

Table A-1: flexural and shear capacity of each slab.

Slab designation	*Critical depth d (mm)*	*P_{all} from flexural capacity (kN)*	*P_{all} from shear capacity (kN)*
S1	*75*	*19.13*	*75.4*
S2	*105*	*26.05*	*105.6*
S3	*45*	*10.76*	*45.26*
S4	*45*	*21.52*	*45.26*
S5	*105 for flexural, 45 for shear*	*52.1*	*45.26*
S6	*75*	*25.51*	*54.8*
S7	*45*	*14.34*	*33*
S8	*45*	*17.2*	*33*
S9	*75*	*36.8*	*75.4*
S10	*45*	*21.52*	*45.26*
S11	*45*	*21.52*	*45.26*

B

Appendix B

MODELLING OF MATERIAL PROPERTIES IN FINITE ELEMENT ANALYSIS

B.1 Introduction

There are three material models for analyzing concrete in ABAQUS: (1) Smeared crack concrete model, (2) Brittle crack concrete model, and (3) Concrete damaged plasticity model. Out of the three concrete crack models, the concrete damaged plasticity model is selected in the present study. Details of the CDP model used in ABAQUS, including the behavior and properties of the concrete and the other material used in this study are described below.

B.2 Concrete Damaged Plasticity in ABAQUS

Concrete damaged plasticity is capable of modelling all structural types of reinforced or unreinforced concrete or other quasi-brittle materials subjected to monotonic, cyclic, or dynamic loads. This model is based on a coupled damage plasticity theory and the multi-axial behaviour of concrete in damaged plasticity model governs by a yield surface, which proposed by **(Lubliner et al.)** [1]. Tensile cracking and compressive crushing of concrete are two assumed main failure mechanisms in this model. Furthermore, the degradation of material for both tension and compression behaviour have been considered in this model. Degradation of concrete in cyclic and dynamic loadings is taken into account by defining two scalar parameters; tensile damage parameter (dt) and compressive damage parameter (dc).

B.2.1 Uniaxial Behaviour of Concrete

Under uniaxial tension, as can be seen in Figure B-1, the stress increases with a linear elastic relationship with strain up to the ultimate tensile strength, and then micro-cracks form microscopically with a tension softening response. There are three different methods to define tension softening response in ABAQUS; stress-strain, stress-displacement or by use of fracture energy, *Gf* [2].

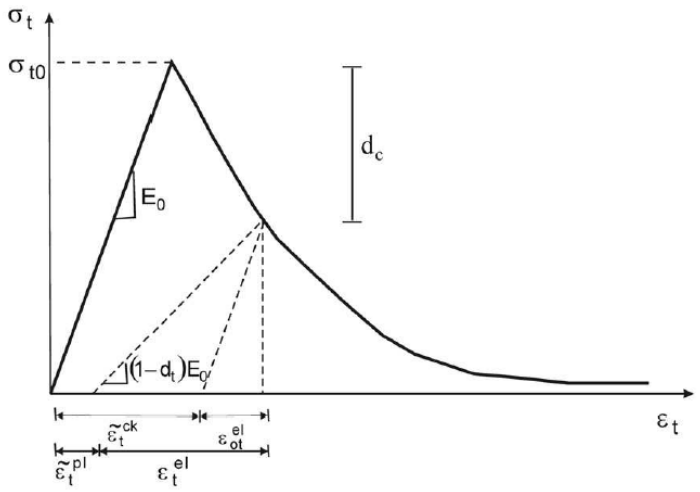

Figure B-1: Uniaxial tensile behaviour of concrete. [3]

To define the tesile stress-strain relation of concrete in ABAQUS, user should input young's modulus (E_0), stress (σ_t), cracking strain ($\varepsilon_t^{\sim ck}$) values and the damage parameter values (*dt*) for the relevant grade of concrete. The cracking strain ($\varepsilon_t^{\sim ck}$) should be calculated from the total strain using Eq. (B-1) below:

$$\varepsilon_t^{\sim ck} = \epsilon_t - \varepsilon_{ot}^{el} \qquad \text{(B-1)}$$

Where, $\epsilon_{ot}^{el} = {}^{\sigma_t}/_{E_o}$, the elastic strain corresponding to the undamaged material, and

$$\varepsilon_c = total\ tensile\ strain$$

In addition, under uniaxial compression, there is a linear elastic relationship between stress - strain until initial yield. After losing stiffness due to bond failure

between the aggregates and the cement paste, the behaviour becomes non-linear. In stresses greater than ultimate strength, stress hardening and strain softening define plastic response. In other words, compressive stress decreases while the corresponding strain increases. The uniaxial compressive behavior of concrete is depicted in Figure B-2.

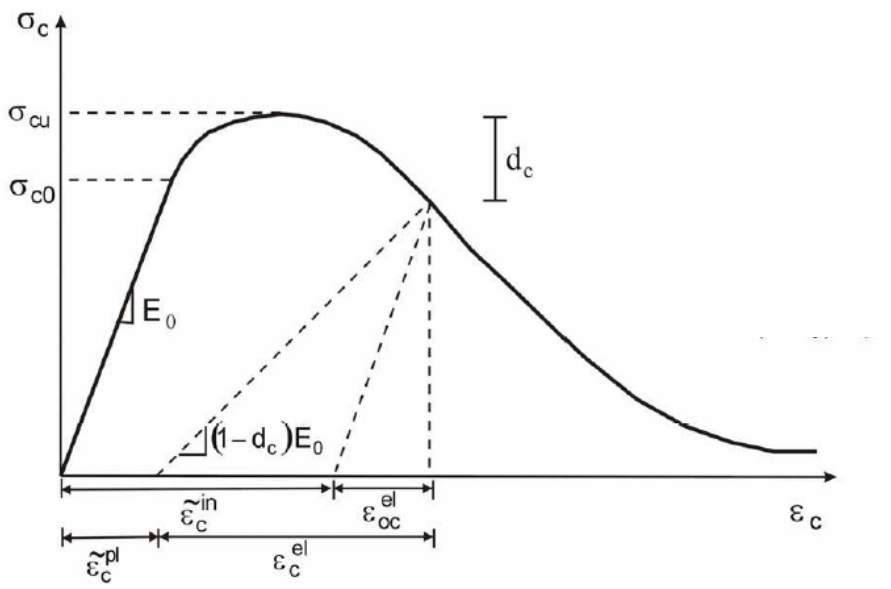

Figure B-2: Uniaxial compressive behaviour of concrete [3]

To define the compression stress-strain relation of concrete in ABAQUS, user needs to enter the stresses (σc), inelastic strains ($\varepsilon_c^{\sim in}$) corresponds to stress values, and damage properties (dc) with inelastic strains in tabular format. Therefore, total strain values should be converted to the inelastic strains using Eq. (B-2):

$$\varepsilon_c^{\sim in} = \epsilon_c - \varepsilon_{oc}^{el} \qquad \text{(B-2)}$$

Where, $\epsilon_{oc}^{el} = {}^{\sigma_c}/_{E_o}$, the elastic compression strain corresponding to the undamaged material, and $\varepsilon_t = total\ compression\ strain$

Compression and tension damage parameters describing crushing and cracking behaviour were defined as tables within CDPM. The following equations developed by **(Birtel and Mark)** [4] were successfully used in obtaining the compression and

damage parameters. Damage parameters take values ranging from 0 (no damage) to 1 (fully damaged), representing the level of damage.

$$d_c = 1 - \frac{\sigma_c E_c^{-1}}{\varepsilon_c^{pl}(1/b_c - 1) + \sigma_c E_c^{-1}} \quad \text{(B-3)}$$

$$d_t = 1 - \frac{\sigma_t E_c^{-1}}{\varepsilon_t^{pl}(1/b_t - 1) + \sigma_t E_c^{-1}} \quad \text{(B-4)}$$

$$\varepsilon_c^{pl} = b_c \, \tilde{\varepsilon}_c^{in} \quad \text{(B-5)}$$

$$\varepsilon_t^{pl} = b_t \, \tilde{\varepsilon}_t^{ck} \quad \text{(B-6)}$$

The coefficients b_c and b_t take values between 0 and 1. Birtel and Mark [4] suggested *bc*=0.7 and *bt*=0.1.

Further, corrective measures should be taken to ensure that the plastic strain values (ε_c^{pl} *and* ε_t^{pl}) calculated using (eq. B-5 and eq. B-6) are neither negative nor decreasing with increased stresses [2].

B.2.2 Concrete Damaged Plasticity Parameters in Triaxial Loading State

In order to describe strength with the equation for triaxial stress as input to the finite element program ABAQUS, a set of five parameters are required to completely describe the plastic behavior of concrete;

Ψ, Dilation angle: The angle of inclination of the failure surface toward the hydrostatic axis, measured in the meridional plane. Physically, dilation angle Ψ is interpreted as a concrete internal friction angle. Maximum value of it equal (56.3°) and minimum value is close to (zero) [5]. Through many trials of geometry with the aim of achieving proper failure to be compatible with the observed experimental failure mechanism, the value of dilation angle was taken as (45°) for beams of both groups.

ϵ: Plastic potential eccentricity, it is a small positive value which expresses the rate of approach of the plastic potential hyperbola to its asymptote. It can be calculated as a ratio of tensile strength to compressive strength. It is recommended to assume $\epsilon = 0.1$ in the CDP model [5].

F_{b0}/f_{c0}: is the proportion of initial equibiaxial compressive yield stress and initial uniaxial compressive yield stress [5]. The default value in ABAQUS is (1.16).

K: is the ratio of the second stress invariant in the tensile meridian to compressive meridian for any defined value of the pressure invariant at initial yield. It is used to define the multi-axial behavior of concrete and is ($0.5<Kc\leq1$) [5]. The default value in ABAQUS is (0.667).

μ: is the viscosity parameter. It does not affect the ABAQUS/Explicit analysis but contribute to converge in an ABAQUS/Standard analysis. According to (Malm) [6] $\mu=10^{-7}$ is recommended because in comparison with characteristic time increment it should be small.

B.3 Material Properties for FEM

B.3.1 Concrete Model Properties

The concrete material parameters in the concrete damaged plasticity model that should be used are: the modulus of elasticity E_0, the Poisson's ratio v and the compressive and tensile strengths of concrete in order to simulate concrete with normal compressive strength, the unconfined stress–strain relationship model for concrete as proposed by **(Popovics)** [7] was used. This relationship based on the concrete cylinder strength, as described in equations (B-7) and (B-8).

$$\frac{f_c}{\hat{f_c}} = \frac{n\times\left[\frac{\varepsilon_c}{\varepsilon_{co}}\right]}{(n-1)+\left[\frac{\varepsilon_c}{\varepsilon_{co}}\right]^n} \qquad \text{(B-7)}$$

$$n = (\,0.4\times10^{-3}\times\hat{f_c}(psi)) + 1.0 \qquad \text{(B-8)}$$

Where:

fc'= the compressive strength of cylinder at maximum stress.

ε_{co}= strain of concrete at maximum stress.

n = a curve-fitting factor.

On the other hand, tensile stress-strain (σ-ε) relationship was assumed linear up to the uniaxial tensile strength and then determined using the exponential function in the equation (B-9) [8].

$$\sigma = f_t \times \left[\frac{\varepsilon_t}{\varepsilon}\right]^{(0.7+1000\varepsilon)} \ , \ \varepsilon_t = \frac{f_t}{E_o} \qquad \text{(B-9)}$$

B.3.2 Steel Reinforcement Model Properties

The required input parameters for material definition of steel bars, includes density, elastic and plastic behaviour. Elastic behaviour of steel material is defined by specifying Young's modulus (Es) and Poisson's ratio (*v*) of which typical values are 200000 MPa and 0.3, respectively. Plastic behaviour is defined in a tabular form, included yield stress and corresponding plastic strain. According to **(Hibbit et al.)** [2] true stress and logarithmic strain should be defined [34]. Input values of stress in each point for an isotropic material are calculated according to Eqs. (B-10) and (B-11). A higher number of input points lead to results that are more accurate.

$$\sigma_{true} = \sigma_{nominal}\ (1 + \varepsilon_{nominal}) \qquad \text{(B-10)}$$

$$\sigma_{in}^{pl} = \ln(1 - \varepsilon_{nominal}) - (\frac{\sigma_{true}}{E_s}) \qquad \text{(B-11)}$$

B.3.3 Steel Plate Model Properties

The steel plates were modelled using an isotropic linear elastic material model by Eq. (B-12) with solid elements for all models. The assumption for the material of loading and supporting plates is to avoid problems in solution due to the large deformations that will be developed or stress singularity in the plates.

$$f_s = E_s \varepsilon_s \ (MPa), \ \ \varepsilon_s \leq \varepsilon_y \qquad \text{(B-12)}$$

References:

1. Lubliner, J., Oliver, J., Oller, S., & Oñate, E. "A plastic-damage model for concrete". International Journal of Solids and Structures, 25(3), pp. (299-326), doi: https://doi.org/10.1016/0020-7683(89)90050-4, (1989).
2. Hibbitt, Karlsson, & Sorensen, "ABAQUS User's Manual". Pawtucket, 6th Edition, (2010).
3. Jankowiak, Tomasz, and Tomasz Lodygowski. "Identification of parameters of concrete damage plasticity constitutive model." *Foundations of civil and environmental engineering*6.1 (2005): 53-69.
4. Birtel, V., and P. Mark. "Parameterised finite element modelling of RC beam shear failure." *ABAQUS users' conference*. 2006.
5. Kmiecik, P., and M. Kamiński. "Modelling of reinforced concrete structures and composite structures with concrete strength degradation taken into consideration." *Archives of civil and mechanical engineering* 11.3 (2011): 623-636.
6. Malm, R., "Shear cracks in concrete structures subjected to in-plane stresses," Lic. thesis, Royal Institute of Technology (KTH) (2006), Stockholm, Sweden.

7. S. Popovics, “A numerical approach to the complete stress-strain curves of concrete,” *Cement and Concrete Research*, vol. 3, no. 5, pp. 583-599, 1973.

8. Dere, Y., & Koroglu, M., A. “Nonlinear FE Modeling of Reinforced Concrete,” International Journal of Structural and Civil Engineering Research, Vol.(6), No.1, pp.(71-74), (2017).

الخلاصة

ان هذا البحث يقدم دراسة عملية وعددية لتأثير المقطع العرضي غير الموشوري على السلوك الإنشائي للبلاطات الخرسانية أحادية الاتجاه تحت تأثير الحمل المتكرر. اشتمل العمل التجريبي على اختبار أحد عشر بلاطة من الخرسانة المسلحة أحادية الاتجاه مقسمة إلى مجموعتين. تتكون المجموعة الأولى من خمس بلاطات ذات فضاء واحد، بينما تتكون المجموعة الثانية من ستة بلاطات ذات فضاءين. تمت دراسة تأثير العوامل الثلاثة على السلوك العام للبلاطات، بما في ذلك: شكل المقطع وحالة الاسناد وعدد الفضاءات.

بالنسبة لبلاطات المجموعة الأولى، كانت إحداها موشورية بعمق ثابت، بينما كانت جميع البلاطات الأخرى غير موشورية مع مقطع عرضي مستدق له عمق متفاوت وحالة اسناد مختلفة بنفس الحجم من الخرسانة وكمية حديد التسليح. تشير النتائج إلى أن سعة التحميل للبلاطة أحادية الاتجاه بإسناد بسيط ذات المقطع المحدب زادت بنسبة 32٪ نسبتا الى البلاطة الموشورية. بينما زادت البلاطة ذات المقطع المقعر بإسناد مثبت بنسبة 68٪

من ناحية أخرى، تتكون بلاطات المجموعة الثانية من ستة بلاطات خرسانية ذات فضاءين بنفس الحجم من الخرسانة. كان اثنان منهم موشوريين بعمق ثابت، بينما المتبقية غير موشوريين مع مقطع عرضي مستدق متفاوت العمق. تشير النتائج إلى أن الألواح الموشورية في جميع حالات الاسناد كانت أكثر صلابة من الألواح غير الموشورية. لقد وجد أن استخدام بلاطة مدببة ذات مقطع مقعر أو محدب له تأثير ضئيل على قدرة التحمل نسبتا الى البلاطة الموشورية. من ناحية أخرى، ان ذلك تسبب في زيادة الهطول عند الاحمال الخدمية مقارنة بالبلاطة الموشورية. وبالتالي، يوصى باستخدام البلاطات الموشورية المستمرة أحادية الاتجاه بدلاً من البلاطات غير الموشورية بسبب الصلابة العالية ونفس القدرة على تحمل الأحمال تقريبًا.

في الجزء الثاني من هذه الدراسة، أجري تحليلا لا خطيا" بالاعتماد على العناصر المحددة ثلاثية الأبعاد لمحاكاة البلاطات الخرسانية المسلحة أحادية الاتجاه من خلال برنامج العناصر المحددة ABAQUS/Standard نسخة (2017). في هذ البرنامج الحاسوبي تم استخدام أنموذج اللدونة للخرسانة المتضررة (Concrete damaged plasticity) وخصائص المواد التي تم الحصول عليها من الفحوصات العملية، شمل هذا التحري آثار متغير مختلف أخر على سلوك البلاطات الخرسانية المسلحة وهو تسليط حمل ثابت بدل الحمل التكراري. لقد قورنت النتائج العددية بالنتائج العملية التي تم الحصول عليها من حيث منحني الحمل – الهطول. لقد أظهرت النتائج أن تحليل العناصر المحددة تنبأ بسلوك البلاطات الخرسانية المسلحة وبتوافق جيد مع البيانات التجريبية حيث كانت الاستجابة العامة لمنحنيات الهطول – مقدار الحمل، والحمل النهائي، والهطول عند اقصى حمل في منتصف الفضاء للبلاطات المسلحة المدروسة والتي تنبأ بها FEM في توافق جيد مع النتائج التجريبية. كان متوسط الفرق في النتائج حوالي 5.9٪ زيادة في الأحمال النهائية، وانخفاض بنسبة 5.37٪ في أقصى انحراف عند أحمال الخدمة، وزيادة 4.1٪ في الحد الأقصى للانحراف عند الأحمال النهائية. عدديًا ، ثبت أن بروتوكول الحمل المتكرر المعتمد تجريبيًا وعدديًا فعال في دراسة التأثير السلبي لتطبيق الحمل المتكرر مقارنة بالحمل الرتيب.

جمهورية العراق
وزارة التعليم العالي والبحث العلمي
جامعة بابل
كلية الهندسة
قسم الهندسة المدنية

سلوك البلاطات الخرسانية المسلحة احادية الاتجاه غير الموشورية تحت تأثير الاحمال المتكررة

رسالة

مقدمة إلى كليَّةِ الهندسة – جامعةِ بابل كجزءٍ مِنْ متطلبات الحصول على درجة الماجستير في الهندسة/ الهندسة المدنية/ هندسة الانشاءات

من قبل

فاطمة نعمة ابراهيم مسير

بكالوريوس علوم في الهندسة المدنية 2017

أشراف

الأستاذ الدكتور: نمير عبد الامير علوش

2022